

Electron-hole exchange interaction for donor-acceptor pairs in CdS determined as a function of separation distance by optically detected magnetic resonance

R. T. Cox and J. J. Davies*

*Groupe de Physique des Semiconducteurs, Service de Physique, Département de Recherche Fondamentale
Centre d'Etudes Nucléaires de Grenoble, Boîte Postale No. 85X,*

38041, Grenoble Cédex, France

(Received 14 July 1986)

This paper describes the first investigation of the way in which the electron-hole exchange interaction for a donor-acceptor pair depends on the separation r between the donor and the acceptor. The case studied is that of shallow donor electrons interacting with shallow acceptor holes in CdS. The electron-hole recombination produces the well-known green edge emission, which is studied here by optically detected magnetic resonance (ODMR) and by time-resolved (TR) luminescence spectroscopy. Coulomb shifts cause the energy of the zero-phonon photoluminescence transition to depend on r , so that pairs of a given separation can be studied selectively by appropriate choice of the observation wave length. The exchange interaction produces line splittings in the ODMR spectra, which give a direct determination of the exchange constant A (the separation between the Γ_6 and Γ_5 levels in zero field) for the particular pairs selected. In this way, values of A between 0.5 and 50 μ eV can be measured. The TR luminescence experiments were conducted in order to establish the relation between observation wave length and the value of r ; they also provided measurements of the radiative recombination rate constant W . The parameters A and W are expected to have the form $A_0 \exp(-2\rho/a_D)$ and $W_0 \exp(-2\rho/a_D)$, respectively, for large values of ρ , where a_D is the donor Bohr radius and ρ is an effective intrapair separation defined by $\rho = r[\sin^2\theta + (\epsilon_{\perp}/\epsilon_{\parallel})\cos^2\theta]^{1/2}$, where θ is the angle between the pair axis and the crystal c axis. Values of A were measured over the range $\rho = 1.5a_D$ to $4a_D$, and values of W for the range $\rho = 4a_D$ to $9a_D$. The data for A at $\rho > 2a_D$ and for W can be fitted by the exponential laws given above, with a common value of $a_D = 2.75$ nm. The parameter $A_0 \simeq 0.85$ meV, and $W_0 \sim 2 \times 10^8$ s $^{-1}$. The value for a_D is in good agreement with the estimate of 2.39 nm obtained from effective-mass theory. From $2a_D$ to $9a_D$, the values of A and W change by 6 orders of magnitude and the results provide one of the best demonstrations ever obtained that the tail of a donor envelope function can be described by a single exponential out to very large distances. For $\rho < 2a_D$, the exchange splitting ceases to follow a simple exponential dependence and, as expected, tends towards the value $A_X = 0.21$ meV of the exchange splitting for the free exciton. However, the departure from the exponential law occurs at values of ρ greater than predicted, indicating the need for improved theories of the electron-hole exchange interaction in semiconductors.

I. INTRODUCTION

The energy levels of a neutral-donor—neutral-acceptor pair in a semiconductor are split by the electron-hole exchange interaction. In the past, investigations^{1,2} of this interaction have been limited to donor-acceptor pairs in which the exchange splitting is large enough to be resolved in the emission spectrum produced when the electron on the donor recombines with the hole on the acceptor. Such observations have therefore been restricted to donors and acceptors which lie close to each other, and it has hitherto not been possible to investigate how the strength of the exchange interaction depends on the distance r between the two centers. The present article provides the first example of such information. We have succeeded in measuring exchange interactions down to the microelectronvolt range using optically detected magnetic resonance (ODMR), a technique which allows determination of the splittings of the magnetic sublevels of a

luminescent excited state even when these splittings are much smaller than the optical linewidth.³

The particular case we have studied is that of shallow donors interacting with shallow acceptors in cadmium sulphide CdS. Here the spin and orbital angular momenta of the hole are coupled in a state $j_h = \frac{5}{2}$ so the spin-exchange interaction appears as a coupling between \mathbf{j}_h and the electron spin \mathbf{s}_e (usually called “ j - j coupling”) which we write

$$\mathcal{H} = a \mathbf{j}_h \cdot \mathbf{s}_e . \quad (1)$$

We have measured the magnitude of the coupling parameter a for donor-acceptor separations from 3 to 10 nm, corresponding to about one to about four times the donor Bohr radius a_D . Over this range, the strength of the interaction is observed to change by 2 orders of magnitude.

For intrapair separations r greater than about $2a_D$, the coupling parameter shows an exponential decrease with increasing r and we can account for the results using a

Heitler-London type description in which the electron-hole wave function is taken to be an (antisymmetrized) product of the isolated donor and isolated acceptor wave functions. A donor envelope function of hydrogenic form proves satisfactory (while the exact form of the much more compact acceptor function is not very significant). For pairs separated by less than about $2a_D$, we find that the measured exchange splittings tend towards the value recently determined for the exchange-induced splitting of the free exciton in CdS.^{4,5} This is as expected, for, in the limit where the opposite charges of the donor and acceptor cores cancel, the trapped electron and hole transform into an exciton. However, the Heitler-London description of the approach to this limit is in disagreement with the data, pointing out the need for a more appropriate, unified theory of exciton and donor-acceptor wave functions.

In the experiments to be described, ODMR signals from donor-acceptor pairs are obtained by monitoring the intensity of the donor-acceptor recombination luminescence. As discussed later, both the wave length and the decay time of the emission are sensitive to the spatial separation between the donor and the acceptor. By suitable selection of the wave length and of the observation time after pulsed excitation, recombination at donor-acceptor pairs within a comparatively narrow range of separations centered at given values of r can be studied. The magnetic resonance signals are split by the j - j coupling and the magnitude of this coupling can thus be determined as a function of intrapair separation.

A brief description of preliminary results of this work has been given previously.⁶ The plan of the present article is as follows. In Sec. II we summarize the relevant features of the CdS emission spectrum. In Sec. III we present a time-resolved luminescence study that was undertaken in order to estimate E_∞ , the emission energy that would correspond to a donor and an acceptor separated by an infinite distance. (The parameter E_∞ had to be determined so that the scale of emission wave lengths used in the ODMR study could be converted to a scale of donor-acceptor separations.) We then consider (Sec. IV) the energy levels for coupled donor-acceptor pairs in a magnetic field and describe the ODMR spectrum and how this is affected by the j - j coupling. In Sec. V the wave length-selected time-resolved ODMR experiments are described and the dependence of the strength of the j - j coupling interaction on the intrapair separation is determined. Finally, in Sec. VI the results are discussed in terms of currently available theory. Some detailed aspects of the analysis are described in the appendixes.

II. SHALLOW-DONOR-SHALLOW-ACCEPTOR RECOMBINATION EMISSION IN CdS

The green edge emission from CdS ranks among the classic examples of luminescence phenomena in semiconductors.^{1,2,7-14} At 2 K it is made up of two overlapping series of bands. Each series consists of a zero-phonon band and a series of LO-phonon replicas spaced at intervals of about 40 meV. One series, referred to as the high-energy series (HES), has its zero-LO-phonon band peaking typically at 512.5 nm (2.419 eV) and is usually attributed

to recombination between conduction-band electrons and holes bound at shallow acceptors. The other series, referred to as the low-energy series (LES), is due to recombination between electrons bound to shallow donors and holes bound to shallow acceptors. The zero-LO-phonon peak wave length for the low-energy spectrum depends on the excitation conditions (see below); under continuous excitation at low power it occurs typically near 517 nm (2.398 eV).

It is the low-energy series that concerns us in the present work. After pulsed excitation, the bands decay nonexponentially and shift with time to longer wave lengths. This behavior, which is characteristic of donor-acceptor recombination, arises because there is a Coulomb interaction between the ionized donor and the ionized acceptor after recombination has occurred. Because of this term, the spectral position of the zero-phonon transition for a recombining donor and acceptor separated by a distance r is¹⁵

$$h\nu = E_G - (E_A + E_D) + \frac{e^2}{4\pi\epsilon_\theta\epsilon_0 r}, \quad (2)$$

where E_G is the bandgap and where E_D and E_A are, respectively, the donor and acceptor ionization energies. The anisotropic dielectric constant ϵ_θ is given by¹⁶

$$\epsilon_\theta^2 = \epsilon_\perp \epsilon_\parallel \sin^2\theta + \epsilon_\perp^2 \cos^2\theta,$$

where θ is the angle between the pair orientation and the crystal's c axis. Additional terms of non-Coulombic form,¹⁵ important only at very small values of r , have been omitted from Eq. (2); as discussed in Sec. V, they are not significant for the pairs we have studied in the present work.

It can be seen from Eq. (2) that pairs with smaller values of r recombine with higher emission energies. Such pairs also recombine more quickly, so that, in a pulsed excitation experiment, as the delay before observation increases, the emission becomes increasingly dominated by contributions from long-lived pairs. It is this that produces the characteristic shift to longer wave lengths. The presence of the distance-dependent decay times and Coulomb shifts is crucial to the success of the methods used to discriminate between pairs of different separations in the ODMR experiments described later.

For small separations, the Coulomb interaction is sufficiently strong and in suitable specimens the linewidths can be sufficiently narrow for the emission lines due to pairs with different discrete values of r to be resolved. Zeeman spectroscopy is then possible and the j - j coupling of pairs with separations thought to be about 1 nm has been studied in this way.^{1,2}

For greater values of r the different pair spectra merge into a continuous distribution of lines. In fact, the emission under continuous excitation is dominated by contributions from the large number of pairs with large separations. These "distant pairs" have been the subject of previous ODMR studies.^{11,17}

A further complication in the emission spectrum can arise through the simultaneous presence of more than one type of shallow acceptor. Different acceptors have

markedly different ionization energies and lead to series of emission bands that are displaced relative to each other.¹¹ For the present investigation we have therefore taken care to select a crystal in which only one dominant type of shallow acceptor, lithium, is present.^{10,11} On the other hand, the differences in ionization energy between different (single) donors are too small to be significant in the present work.

III. TIME-RESOLVED OPTICAL SPECTROSCOPY

Of crucial importance to the interpretation of the ODMR results to be described later is the relationship between the zero-phonon emission energy E and the intrapair separation. From Eq. (2) we can write

$$E = E_{\infty} + \frac{e^2}{4\pi\epsilon_0\rho}, \quad (3)$$

where $E_{\infty} = E_G - (E_A + E_D)$ is the value of E for infinitely large separation. We have replaced the anisotropic dielectric constant ϵ_{θ} by a quantity $\epsilon = (\epsilon_{\parallel}\epsilon_{\perp})^{1/2}$ and the separation r by an effective separation ρ , where

$$\rho = r [\sin^2\theta + (\epsilon_{\perp}/\epsilon_{\parallel})\cos^2\theta]^{1/2}, \quad (4)$$

so that $\epsilon\rho = \epsilon_{\theta}r$. In terms of the effective separation ρ , the Coulomb interaction is isotropic; the other consequences of using ρ rather than r are discussed in Appendix A. Following Flohrer *et al.*,¹⁸ we shall use the values $\epsilon_{\parallel} = 8.92$ and $\epsilon_{\perp} = 8.42$ obtained from infrared reflectivity measurements¹⁹ so that $\epsilon = 8.67$. Note that the reported values of the ratio $\epsilon_{\perp}/\epsilon_{\parallel}$ range from 0.92 to 0.94 (see Appendix A) so that the maximum difference between ρ and r is only $\sim 4\%$.

The essential problem in our work is to determine the value of E_{∞} for the particular donor-acceptor combination studied, since the effective donor-acceptor separation ρ can then be deduced from the emission energy over the range of validity of Eq. (3). In principle, E_{∞} can be obtained from values of E_G , E_A , and E_D , but these quantities are not known to sufficient accuracy. To determine E_{∞} we have therefore studied the shift of the emission energy as a function of time delay after an excitation pulse. This shift occurs because the recombination rate depends on the effective separation ρ . The present section describes these experiments and shows how a value of E_{∞} may be obtained by an analysis that is essentially equivalent to extrapolating the results to infinite delay time.

The usual method of obtaining time-resolved luminescence spectra is to use a gated detector to measure the intensity of luminescence at a delay time t_D after an excitation pulse. This discriminates against centers having a characteristic decay time much shorter or much longer than t_D . However, Dunstan and co-workers^{20,21} have recently pointed out that such experiments can give quite misleading results if the pulse sequence is repeated with some period T not very much greater than t_D , as often must be done to improve the signal-to-noise ratio. Then the population of centers with lifetimes longer than T will build up to a high level during successive pulses and may contribute a nonnegligible background to the signal

detected. A technique called frequency-response spectroscopy (in-quadrature detection of the synchronous signal component induced by a sinusoidally modulated excitation source) has been used to avoid this problem.²¹ However, we prefer to keep pulsed excitation and a gated detector as in the usual time-resolved spectroscopy technique (because this gives high contrast against short-lived species), but we use the modified observation sequence shown in Fig. 1.

We place two observation gates after every laser pulse and extract the *difference* between the two integrated intensities by means of a phase-sensitive detector; see Fig. 1. This sequence discriminates against short-lived pairs because they decay before the first observation gate and against long-lived pairs because their intensity cannot vary very much between the first and second gates.

Our excitation source was an argon laser operated at 496 nm, pulsed by an acousto-optic deflector. The emission was observed with a gated photomultiplier (EMI 9816G) with the two gate pulses spaced $T/2$ apart, where T is the laser period. Emission spectra were recorded as a function of wave length for laser pulse repetition rates from 100 kHz to 1 Hz. The sample was immersed in pumped liquid helium at about 2 K.

Two examples of time-resolved emission spectra recorded in this way are shown in Fig. 2. A shift of the spectrum as the repetition rate decreases is readily apparent. It occurs because the longer-lived pairs have smaller Coulomb energies. The peaks in Fig. 2 also narrow slightly when the repetition rate decreases because the *spread* of Coulomb energies becomes smaller. At the lowest repetition rates used (1 Hz), Coulomb broadening is negligible and the origin of the residual linewidth ΔE of about 0.010 eV (full width at half maximum) is not obvious. Moroz *et al.*¹² have attributed the broadening to interaction with transverse-optical phonons.

In our experiments we measure E_{peak} , the peak energy of the zero-LO-phonon line, but in the analysis we need to

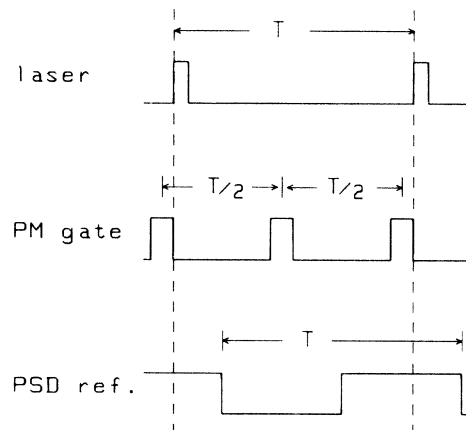


FIG. 1. Sequence of pulses applied to the laser modulator, photomultiplier gate, and phase-sensitive detector reference in the time-resolved luminescence measurements. Here and in Fig. 6 a positive-going pulse switches on the appropriate device.

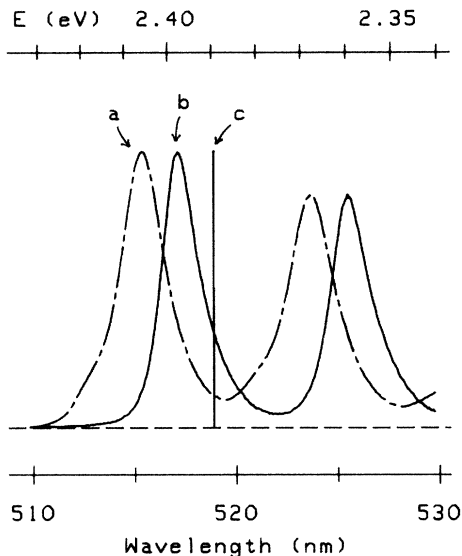


FIG. 2. Time-resolved luminescence spectra from a CdS crystal excited by 496 nm radiation at 2 K, showing the zero-LO- and first-LO-phonon peaks. The spectra are obtained with the pulse sequence of Fig. 1 with repetition rate $1/T$ set at 10^5 Hz in *a* and at 10 Hz in *b*. The vertical axis represents luminescence intensity per unit wavelength interval and the two spectra have been normalized to the same maximum peak height. The vertical line *c* marks $E_{\infty \text{ peak}}$, the position of the zero-LO-phonon peak for infinite intrapair separation.

remember that this is shifted to lower energy (by about 3.5 meV according to the analysis of Moroz *et al.*¹²) with respect to the true zero-phonon energy appearing in Eq. (3). Deduction of $E_{\infty \text{ peak}}$ (the peak energy for infinite intrapair separation corresponding to infinite lifetime) from these measurements requires a theory of the radiative transition probabilities in a system of donor and acceptor centers. We shall use the simplest theory, the "isolated-pair" model, in which it is assumed that each trapped electron recombines with the nearest trapped hole and that the energy and transition probability of this event are unaffected by the presence of other centers in the vicinity.

The theory of the transition probability for recombination at an isolated pair in an isotropic crystal has been given by many authors (e.g., Refs. 15 and 22) and needs only slight modification for the case of CdS, which has the wurtzite structure. For a hydrogenic donor wave function of radius much greater than the acceptor radius, the recombination rate is

$$W = W_0 \exp(-2\rho/a_D), \quad (5)$$

where W_0 is a constant proportional to the conduction band to valence-band transition matrix elements. Here, we have replaced the donor-acceptor separation r by our effective separation ρ [Eq. (4)] and a_D is an effective Bohr radius for the donor given by $4\pi\epsilon_0\hbar^2/e^2m_e$, where m_e is the electron effective mass defined in Appendix A. We justify these substitutions in Appendix A where we show that in CdS the donor wave function is very close to

spherical in ρ space. This is important because it means that there is close to a one-to-one correspondence between the pair Coulomb energy and its radiative decay rate even in the anisotropic crystal. Combining Eqs. (5) and (3) gives

$$\ln \left(\frac{W}{W_0} \right) = - \frac{e^2}{2\pi\epsilon_0 a_D} \frac{1}{(E_{\text{peak}} - E_{\infty \text{ peak}})}. \quad (6)$$

where we have replaced $(E - E_{\infty})$ by $(E_{\text{peak}} - E_{\infty \text{ peak}})$. Measurements of W can thus in principle be used to determine $E_{\infty \text{ peak}}$, and also a_D .

The response of our measurement sequence (Fig. 1) at repetition frequency $1/T$ is maximum for pairs with recombination rate W equal to $1/(\xi T)$, where ξ depends on the degree of saturation, as discussed in Appendix B. For example, for low excitation power (no saturation), $\xi=0.39$; in this case the response falls to half its maximum for $W=1/(0.167 T)$ and for $W=1/(1.50 T)$, and on a logarithmic scale is about a decade wide (which is of the same order as the width of the response function in frequency-response spectroscopy,²¹ a broad response function being inevitable in any kind of time-resolved spectroscopy). A decade change in W corresponds approximately to a change of one donor Bohr radius in the separation parameter ρ (irrespective of the value of ρ). Thus the experiment is most sensitive to pairs with separations within a range of about $\pm a_D/2$ centered on the value of ρ that corresponds to a value of W near $(\xi T)^{-1}$.

If we make the simplifying assumption that E_{peak} , the peak energy in the time-resolved emission spectrum, corresponds to pairs with this value of W , a plot of $\ln(T^{-1})$ against $(E_{\text{peak}} - E_{\infty \text{ peak}})^{-1}$ should, for the correct choice of $E_{\infty \text{ peak}}$, produce a straight line [Eq. (6)]. The parameters $E_{\infty \text{ peak}}$, ϵa_D , and W_0 can therefore be determined successively, as follows, from a graph of $\ln(1/T)$ against the corresponding experimentally determined values of $(E_{\text{peak}} - E_{\infty \text{ peak}})^{-1}$. The value of $E_{\infty \text{ peak}}$ is chosen to make the data lie as closely as possible on a straight line. The value of ϵa_D is then given by the gradient of this line. An estimate of W_0 is obtained by setting W_0 equal to $(1/\xi T_0)$ where T_0^{-1} is the value of T^{-1} at the intercept of the straight line with the axis at $(E_{\text{peak}} - E_{\infty \text{ peak}})^{-1} = 0$ (this value of W_0 has to be revised, however, in view of the discussion later in this section).

In Fig. 3, we show such a graph, plotted for $\lambda_{\infty \text{ peak}} = 518.90$ nm ($E_{\infty \text{ peak}} = 2.389$ eV). The straight line gives an excellent fit to the data over almost 4 orders of magnitude of T ; only the data points at the highest repetition rates lie away from this line. Values of $\lambda_{\infty \text{ peak}}$ less than 518.8 nm or greater than 519.0 nm give graphs with marked curvature at both high and low repetition rates.

The argument presented above is oversimplified for two reasons. First, it makes no allowance for the considerable width ΔE of the zero-phonon emission, which causes a large overlap of the emission bands for pairs of different values of W , and, second, it assumes that the distribution of pair separations $n(\rho)$ is flat, i.e., that it is independent of ρ . We have already noted that the experiment detects

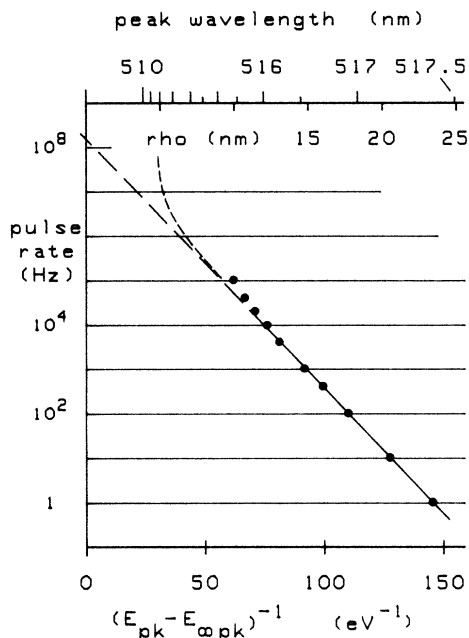


FIG. 3. Relationship between the observed values of the peak energy E_{peak} of the zero-LO-phonon transition and the repetition rate ($1/T$) of the pulse sequence used in the time-resolved luminescence measurements. The data are plotted on a scale of $(E_{\text{peak}} - E_{\infty \text{ peak}})^{-1}$ for the particular choice $E_{\infty \text{ peak}} = 2.3894$ eV ($\lambda_{\infty \text{ peak}} = 518.9$ nm), which, under the assumptions made in the text, is also a linear scale of effective intrapair separation ρ . The straight line is drawn to give the best fit to the data at low pulse rates. The curve represents values given by the simulation procedure of Appendix B, with $a_D = 2.55$ nm, $W(0) = 2.0 \times 10^8$ s $^{-1}$ and with the excitation rate proportional to $n(\rho)$.

decay rates over a rather wide range. Since the number of pairs of a given separation ρ is in reality a rapidly increasing function of ρ , the density of pairs with given W changes appreciably within the range of values of ρ spanned by the response function. This skews the response towards smaller values of W (larger ρ).

These effects are analyzed in Appendix B, and are more pronounced for small values of ρ , where the dependence of $(E_{\text{peak}} - E_{\infty \text{ peak}})^{-1}$ is predicted to depart from the straight line of the simplified theory, as shown by the calculated curve in Fig. 3. The calculated deviation occurs, however, at values of $1/T$ that are higher than those at which the experimental data begin to deviate markedly from the straight line. A possible explanation of the anomalous deviation of the data in terms of the effects of the donor-acceptor exchange interaction is discussed at the end of Appendix B. In view of this explanation, we do not think that the anomaly negates the validity of our analysis for the rest of the data range. Therefore, we retain a value $\lambda_{\infty \text{ peak}} = 518.9 \pm 0.1$ nm, i.e., $E_{\infty \text{ peak}} = 2.3894 \pm 0.0005$ eV. Taking the estimate by Moroz *et al.*¹² of the effect of TO-phonon broadening, we deduce the true zero-phonon energy parameter for our system ($= E_{\infty \text{ peak}} + 3.5$ meV) to be 2.393 eV.

The value of ϵa_D obtained from the fit in Fig. 3 is 22.1 nm, so that, with $\epsilon = 8.67$, we find $a_D = 2.55$ nm. The data points (at large T) fit straight lines of progressively changing slope for choices of $\lambda_{\infty \text{ peak}}$ ranging from 518.8 to 519.0 nm; the corresponding estimates of a_D range from 2.85 nm to 2.30 nm, respectively. As mentioned earlier, values of $\lambda_{\infty \text{ peak}}$ outside this range do not yield a satisfactory straight-line plot, so we conclude that $a_D = 2.55 \pm 0.3$ nm.

This is close to the value of 2.39 nm calculated from the formula $a_D = \epsilon a_0 / m_e$ given by effective mass theory, where a_0 is the Bohr radius for the hydrogen atom and where m_e is the appropriately averaged electron mass, taken to be $0.192 m_0$ (see Appendix A). (It is interesting to note that with a slightly different choice of ϵ , i.e., 8.95, our experimental value of ϵa_D and the effective mass formula would give identical values of 2.47 nm for a_D .)

We emphasize that, since $\rho \propto (E_{\text{peak}} - E_{\infty \text{ peak}})^{-1}$ [see Eq. (3)], the horizontal scale of Fig. 3 is also, for the correct choice of $E_{\infty \text{ peak}}$, a linear scale of the intrapair separation ρ . The values of ρ for $E_{\infty \text{ peak}} = 2.3894$ eV and $\epsilon = 8.67$ are shown at the top of the diagram.

According to the simplified theory, the intercept (at ~ 8.1) of the straight line with the vertical axis in Fig. 3 should correspond to $\log_{10}(W_0 \xi)$. However, the calculations discussed in Appendix B, which allow for the finite line broadening ΔE and for the effect of the pair distribution function, show that, for our donor-acceptor system, the straight line that fits the data for $(1/T)$ in the $1-10^4$ Hz range intercepts the axis at $\log(0.8 W_0)$. That is, the effective value of ξ in our case is 0.8 instead of 0.39. (In view of such effects, which are inevitable in time-resolved or frequency-response spectroscopy of pair recombination, extrapolated values of W_0 should be interpreted with caution.) We find from our analysis that $W_0 = 2.0 \times 10^8$ s $^{-1}$. There is a large uncertainty of the order of a factor of 2 in this figure because we are extrapolating from data points corresponding to values of W much smaller than W_0 . [It should perhaps be emphasized that W_0 does not in reality represent the limit of the recombination rate constant as $\rho \rightarrow 0$ since Eq. (5) will be incorrect at small values of ρ because of effects similar to those discussed in Sec. VI.]

A detailed time-resolved spectroscopic study of the pair recombination emission from CdS has also recently been carried out by Moroz *et al.*¹² In analyzing their data, these authors used known values of E_G and E_A and took E_D to be a variable parameter. Since $E_{\infty \text{ peak}} = E_G - (E_A + E_D) - 3.5$ meV, this is essentially equivalent to the present approach, in which we varied $E_{\infty \text{ peak}}$ to obtain the best straight line at large values of $(E_{\text{peak}} - E_{\infty \text{ peak}})^{-1}$ in Fig. 3. Moroz *et al.* found values of W_0 in the range between 3×10^7 s $^{-1}$ and 1×10^8 s $^{-1}$ and values of a_D between 2.64 and 3.04 nm (we have reevaluated their data with $\epsilon = 8.67$ instead of 8.5). These results are consistent with our own, but a detailed comparison is difficult to make because the combination of donors and acceptors in our crystal may differ from those in the specimens of Moroz *et al.*

It is of interest to recall here the earlier work of Colbow,⁸ who also carried out time-resolved studies of the pair luminescence in CdS. Colbow took E_D to be a vari-

able parameter and from data at delay times between 0.5 ms and 1 s he estimated $W_0 = (4 \pm 2) \times 10^8 \text{ s}^{-1}$. Our present estimate for W_0 thus lies between that of Colbow and those of Moroz *et al.*

The results of this section can now be summarized as follows. For intrapair separations from $\sim 5a_D$ to $\sim 9a_D$, the decay rate of the shallow-donor–shallow-acceptor pairs in our crystal of CdS can be described satisfactorily by an equation of the form $W = W_0 \exp(-2\rho/a_D)$, with $W_0 \sim 2 \times 10^8 \text{ s}^{-1}$ and with $a_D = 2.55 \pm 0.3 \text{ nm}$. The value of the parameter $\lambda_{\infty \text{ peak}}$ was found to be $518.9 \pm 0.1 \text{ nm}$. More precisely, our estimates of a_D and of $\lambda_{\infty \text{ peak}}$ are interrelated: They range from $a_D = 2.85 \text{ nm}$, $\lambda_{\infty \text{ peak}} = 518.8 \text{ nm}$ to $a_D = 2.30 \text{ nm}$, $\lambda_{\infty \text{ peak}} = 519.0 \text{ nm}$. Determination of $\lambda_{\infty \text{ peak}}$ now makes it possible to establish an accurate scale of the intrapair separation ρ in terms of the emission wave length that is being monitored. This scale will be used to analyze the exchange interaction data of Sec. V and should be reliable over the range of separations for which Eq. (3) is valid; as discussed near the end of Sec. V, this should be the case for values of ρ as small as one donor Bohr radius.

IV. THE PAIR ENERGY LEVELS IN A MAGNETIC FIELD

In this section we introduce the effects of the Zeeman interaction and of the exchange interaction. We shall first consider the effect of the magnetic field on the energy levels of donors and acceptors that are well separated, so that the exchange coupling is vanishingly small. We shall then discuss the effects of a finite exchange interaction on the energy levels and on the ODMR spectrum.

A. Isolated donors and acceptors

For CdS, an electron trapped at an isolated donor has a spin $S = \frac{1}{2}$ and the corresponding magnetic-resonance spectrum can be described in the usual notation by a spin Hamiltonian:

$$\mathcal{H}^D = g_{\parallel}^D \mu_B S_z B_z + g_{\perp}^D \mu_B (S_x B_x + S_y B_y), \quad (7)$$

where z is along the crystal axis and $g_{\parallel}^D = 1.7877$, $g_{\perp}^D = 1.7720$.^{11,23}

The shallow acceptor states are more complicated and can be considered in terms of a quasicubic approximation in which the wurtzite crystal is considered as a strained zinc-blende structure. In cubic zinc-blende semiconductors the valence band is split by spin-orbit coupling into an upper, fourfold degenerate band ($J = \frac{3}{2}$) and a lower, twofold degenerate band ($J = \frac{1}{2}$). In the hexagonal structure, the upper valence band is split further into two components A and B , with $J_z = \pm \frac{3}{2}$ and $J_z = \pm \frac{1}{2}$, respectively, separated by about 16 meV.²⁴ The effective Hamiltonian for a hole in the shallow-acceptor states derived from the A and B valence-band edges is thus

$$\mathcal{H}^A = D [J_z^2 - \frac{1}{3} J(J+1)] + g^A \mu_B \mathbf{B} \cdot \mathbf{J}, \quad (8)$$

with $J = \frac{3}{2}$ and $2D = 16 \text{ meV}$.

The large value of D means that in thermal equilibrium

at helium temperatures only the $J_z = \pm \frac{3}{2}$ states are populated. When $D \gg g^A \mu_B B$ the magnetic properties of the $\pm \frac{3}{2}$ states can be described by a formalism in which the effective spin is $S^{\text{eff}} = \frac{1}{2}$ and the effective spin Hamiltonian is

$$\mathcal{H}^{\text{eff}} = g_{\parallel}^{\text{eff}} \mu_B S_z^{\text{eff}} B_z + g_{\perp}^{\text{eff}} \mu_B (S_x^{\text{eff}} B_x + S_y^{\text{eff}} B_y), \quad (9)$$

where $g_{\parallel}^{\text{eff}} = 3g^A$ and $g_{\perp}^{\text{eff}} = 0$. The zero value of g_{\perp}^{eff} implies that magnetic resonance transitions within the $S^{\text{eff}} = \frac{1}{2}$ doublet are forbidden. For the field exactly parallel to the c axis this indeed turns out to be so, but away from the c axis the magnetic field mixes the $J_z = \pm \frac{3}{2}$ states with those for $J_z = \pm \frac{1}{2}$ and magnetic-resonance transitions become allowed.¹¹

The recombination between a shallow-donor electron and a shallow-acceptor hole is represented by the energy-level diagram shown in Fig. 4(a), which applies to a pair with $r \rightarrow \infty$ (so that j - j coupling effects are vanishingly small) with the magnetic field along the crystal c axis. The selection rules for radiative recombination²² are

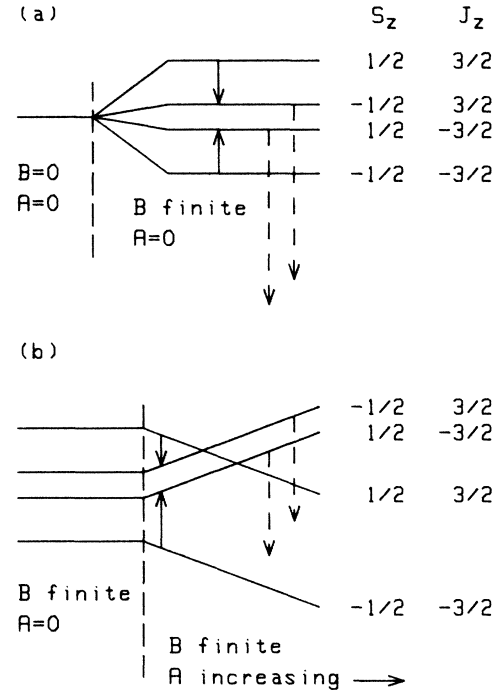


FIG. 4. Effects of magnetic field B and of an exchange splitting A on the four sublevels of a neutral-donor–neutral-acceptor pair in CdS. In (a), application of the field B removes the fourfold degeneracy. The effect of increasing the exchange interaction while keeping B constant is shown in (b). The two magnetic resonance transitions that correspond to inversion of the donor spin are shown as solid arrows; they are degenerate in (a) and split by the exchange in (b). The dashed arrows represent the allowed radiative recombination transitions that transform D^0, A^0 to D^+, A^- . For slow spin relaxation, levels $|\pm \frac{1}{2}, \pm \frac{3}{2}\rangle$ become much more highly populated than levels $|\pm \frac{1}{2}, \mp \frac{3}{2}\rangle$ and both magnetic resonance transitions of the donor produce increases in emission intensity.

shown in the diagram. Since the emission rate depends on the relative orientation of the donor and acceptor effective spins, the possibility arises of changing the emission intensity by changing the spin distribution in the excited states, for example by magnetic resonance. It is this that makes the ODMR experiment possible.

For the crystals used in the present study, the thermalization times within the four excited-state sublevels shown in Fig. 4 are long compared to the recombination times,¹¹ so that the relative populations of the four sublevels are determined by the relative strengths of the recombination processes. The states $|-\frac{1}{2}, -\frac{3}{2}\rangle$ and $|+\frac{1}{2}, +\frac{3}{2}\rangle$ in Fig. 4 thus become more heavily populated than $|-\frac{1}{2}, +\frac{3}{2}\rangle$ and $|+\frac{1}{2}, -\frac{3}{2}\rangle$. Magnetic resonance of either the donor or the acceptor transfers some of this excess population to the emitting states, with a consequent detectable increase in emission intensity.

As already noted, the emission spectrum under continuous laser emission is dominated by contributions from pairs with large values of r . Such pairs have been studied in previous ODMR experiments^{11,17} and donor signals were obtained corresponding to the spin Hamiltonian of Eq. (7). The acceptor signal (obtained only when the magnetic fields was away from the c axis) had g values that depended on the nature of the particular acceptor involved. For the present investigation care was taken to select a crystal in which only one type of acceptor could be detected by ODMR, namely lithium with $|g_{\parallel}^{\text{eff}}| = 2.829 \pm 0.007$.¹¹ The crystal, which was used for both the emission spectroscopy (Sec. III) and the ODMR (Sec. V) was a high-purity sample obtained from the Eagle Picher Corporation.

B. The effects of j - j coupling on the ODMR spectrum

When the electron-hole exchange interaction is introduced, there is a coupling between the acceptor angular momentum $J = \frac{3}{2}$ and the donor spin $S = \frac{1}{2}$ having the form of Eq. (1). The effective Hamiltonian for the pair takes the form¹

$$\mathcal{H}^P = \mathcal{H}^D + \mathcal{H}^A + a\mathbf{J} \cdot \mathbf{S} + \mathcal{H}_c. \quad (10)$$

Hamiltonians \mathcal{H}^D and \mathcal{H}^A have already been defined in Eqs. (7) and (8) and \mathcal{H}_c represents any change in the crystal field at the acceptor arising because of the proximity of the donor. The term \mathcal{H}_c was important in the work of Henry *et al.*¹ on very close pairs, but we shall ignore it in discussing our own measurements on pairs that have relatively large intrapair separations.

The principal objective of our measurements is to determine the coupling parameter a of Eq. (10). (Note that our parameter a is $2a_j$ where a_j is the coupling parameter used in the effective Hamiltonian of Henry *et al.*¹) The value of a depends on the overlap between the electron and hole wave functions and, hence, increases as the intrapair separation gets smaller. We shall see later, however, that a is always much smaller than the splitting $2D$ between the $J_z = \pm \frac{3}{2}$ and $J_z = \pm \frac{1}{2}$ acceptor states. The acceptor states are therefore not significantly mixed by the j - j coupling (e.g., by terms such as $J_+ S_-$) nor are they strongly mixed by the Zeeman interaction (since

$g^A \mu_B B \ll 2D$). The acceptor states thus remain eigenstates of J_z irrespective of the pair separation and irrespective of the direction and value of the magnetic field in our experiments (provided that \mathcal{H}_c remains small).

The energy levels of a donor-acceptor pair when the magnetic field is along the crystal c axis are now

$$E(\pm \frac{3}{2}, \pm \frac{1}{2}) = \pm 3g^A \mu_B B / 2 \pm g_{\parallel}^D \mu_B B / 2 + 3a / 4, \quad (11a)$$

$$E(\pm \frac{3}{2}, \mp \frac{1}{2}) = \pm 3g^A \mu_B B / 2 \mp g_{\parallel}^D \mu_B B / 2 - 3a / 4, \quad (11b)$$

where $\pm \frac{3}{2}$ refers to J_z and $\pm \frac{1}{2}$ to the donor spin projection S_z .

The magnetic-resonance transitions of the donor now occur at field values which satisfy the equation

$$h\nu = g_{\parallel}^D \mu_B B \pm 3a / 2,$$

where ν is the microwave frequency, so that the donor resonance is split into two components, as shown in Fig. 4(b). In a field swept experiment at constant ν , these components are separated in field by

$$\Delta B = 3a / g_{\parallel}^D \mu_B \quad (c \text{ axis}). \quad (12a)$$

Similarly, the (forbidden) acceptor resonance is split by

$$\Delta B' = a / g^A \mu_B. \quad (12b)$$

We note in passing that the present case, in which a donor angular momentum of $\frac{1}{2}$ is coupled to an acceptor angular momentum of $\frac{3}{2}$ in the presence of a strong hexagonal crystal field, is quite different from previous ODMR studies of strongly coupled donor-acceptor pairs, in which donor and acceptor angular momenta both of value $\frac{1}{2}$ have been coupled [e.g., donor-deep-acceptor pairs in ZnS (Ref. 25)]. In the latter case the field splitting of the resonance signals depends nonlinearly on the strength of the exchange coupling and, in the limit of strong coupling, a single resonance line is obtained at the mean of the donor and acceptor g values²⁵ (this line may in some cases be split further by anisotropic exchange²⁶). In the present case, by contrast, the splittings described by Eqs. (12) are linear in field, provided the Zeeman interaction remains small compared to the hexagonal-field splitting.

When the magnetic field is directed along an axis ζ which makes an angle θ with the c axis the j - j splitting of the energy levels is reduced because (for small a) the donor spin states are quantized approximately along ζ , whereas the acceptor states remain eigenstates of J_z , that is remain quantized along the c axis [provided the zero-field splitting $2D \gg g^A \mu_B B$ in Eq. (8)]. For values of $a \ll g^A \mu_B B, g^D \mu_B B$, the energies now become

$$E'(\pm \frac{3}{2}, \pm \frac{1}{2}') \simeq \pm (3g^A \mu_B B \cos \theta) / 2 \\ \pm g_{\parallel}^D \mu_B B / 2 + (3a / 4) \cos \theta,$$

$$E'(\pm \frac{3}{2}, \mp \frac{1}{2}') \simeq \pm (3g^A \mu_B B \cos \theta) / 2 \\ \mp g_{\parallel}^D \mu_B B / 2 - (3a / 4) \cos \theta,$$

where $\pm \frac{1}{2}'$ refers to the values of the donor spin S and where

$$(g^D)^2 = (g_{\parallel}^D)^2 \cos^2 \theta + (g_{\perp}^D)^2 \sin^2 \theta.$$

The donor magnetic resonance now consists of a pair of lines centered at $h\nu/g^D\mu_B$ and split in field by an amount

$$\Delta B \simeq 3a \cos \theta / g^D \mu_B, \quad (13)$$

whereas the acceptor line splitting (although reduced when expressed in energy units) remains equal to $a/g^A\mu_B$ in a field-swept spectrum.

The discussion above has shown how the exchange interaction affects the Zeeman levels of the donor-acceptor pair in CdS. However, when discussing the results of high-resolution photoluminescence studies,^{1,2} it is more convenient to begin with the exchange-coupled energy levels in zero magnetic field. For $B=0$, the Γ_7 donor and Γ_9 acceptor (in the hexagonal point group labeling) are coupled to give two doublets of symmetry Γ_6 and Γ_5 , separated in energy by

$$A = E(\Gamma_5) - E(\Gamma_6) = -3a/2. \quad (14)$$

[Note that Eq. (A4) in Ref. 1 should read $A = -2a_J \langle \phi_{3/2} | J_z | \phi_{3/2} \rangle$.] When a magnetic field B is applied parallel to the c axis, from Eq. (11a) and (11b) the doublets split linearly as shown in Fig. 5. The figure also shows the "donor" magnetic-resonance transitions, that is it shows the energy intervals that would correlate with the donor transitions as $A \rightarrow 0$.

As mentioned in Sec. II, very narrow zero-phonon lines (i.e., lines involving neither LO- nor TO-phonon emission), corresponding to discrete pairs having small r , are sometimes resolved in the luminescence spectrum of CdS. For some of these the effects of exchange are large enough to be resolved and Henry *et al.*¹ and Reynolds and Collins² found that for most such pairs the Γ_5 level was in fact already split in zero-field. This splitting was attributed to a lowering of the symmetry of the acceptor site due

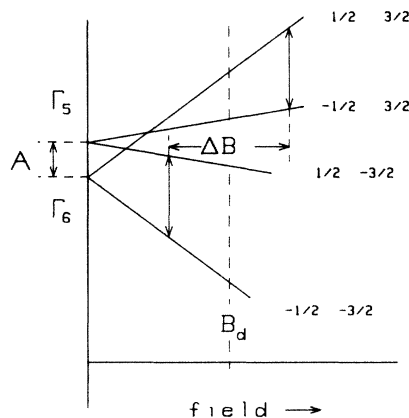


FIG. 5. Effect of a magnetic field applied parallel to the c axis on the Γ_5 and Γ_6 energy levels of an exchange-coupled donor-acceptor pair in CdS. The transitions shown correspond to magnetic resonance of the donor spin and are separated by $\Delta B = 2A/g_D\beta$. For vanishingly small exchange ($A \rightarrow 0$), the transitions would coincide at the resonance field B_d of the isolated donor.

to the presence of the nearby donor, that is to the combined effects of the j - j coupling and of the perturbation \mathcal{H}_c in Eq. (10). In analyzing their data Henry *et al.* introduced a parameter A which equals the energy difference in zero magnetic field between the Γ_6 level and the centroid of the split Γ_5 levels. This parameter is equal to the parameter A used in the present work [Eq. (14)] provided that the perturbation \mathcal{H}_c is not too large. Henry *et al.* found that their values of A were independent of the pair orientation (within the rather large measurement uncertainty set by the optical linewidths). For the restricted range of pair lines that they could study, which corresponded to values of r of about 1 nm (see Sec. VI), their parameter A was about 0.20 meV. No dependence of A on r could be determined in their work. In the present investigation, we are concerned with rather larger values of r , for which complications introduced by symmetry-reducing effects ought to be small.

V. THE ODMR SPECTRA

For the ODMR experiments, the sample was immersed in liquid helium at about 2 K inside an 8.7 GHz microwave cavity having an optical window. The emission was excited by 496 or 488 nm light from an argon laser. The ODMR spectrometer operated in a time-resolved mode²⁷ using the pulse sequence shown in Fig. 6. The laser is pulsed with a repetition period $T/2$. The photomultiplier is switched to the active state after a delay time t_D . During alternate photomultiplier gate pulses, the microwaves are applied. The difference in photomultiplier output between alternate gates is detected by a lock-in system referenced to the period T . In this way one obtains an ODMR spectrum with time discrimination.

The four excited-state sublevels in Fig. 4 are characterized by two decay times τ_r and τ_{nr} for radiative and non-radiative (or, more realistically, radiative and less radiative) levels, respectively. Pairs for which both τ_r and τ_{nr}

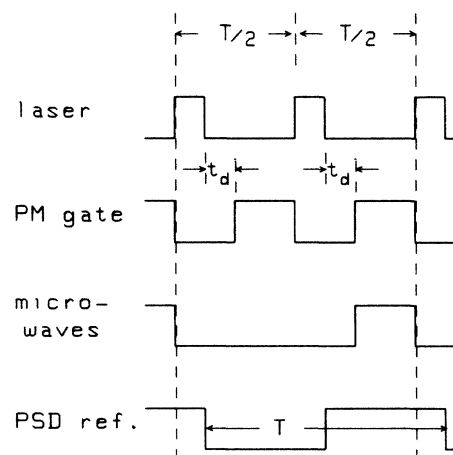


FIG. 6. Pulse sequence used in the time-resolved ODMR experiment. As in Fig. 1, a positive-going pulse switches on the appropriate device.

are much smaller than the delay time t_D are not detected. Similarly, pairs for which these decay times are much longer than the cycle time T cannot contribute a strong signal at the detection frequency $1/T$. The system has optimum sensitivity for pairs with τ_r of order t_D or smaller but with $\tau_{nr} > t_D$. For such pairs, the radiative decay occurring during the delay period t_D leaves a substantial population difference between the two types of sublevels, and the subsequent microwave pulse can induce a large population transfer. We vary the system response simply by varying the overall repetition rate of the pulse sequence of Fig. 6.

We first discuss ODMR spectra obtained by monitoring the whole of the donor-acceptor recombination emission: Here we simply use broad-band optical filters to pass the green emission and to block scattered laser light and any emission of wavelength greater than 600 nm (in this way, we suppress troublesome ODMR signals from deep centers, including the copper centers described in Ref. 26, which are unrelated to the present study). A typical series of ODMR spectra for different repetition periods T is shown in Fig. 7. Here the magnetic field B is oriented along a direction close to the c axis (but not exactly along c , in order that the acceptor ODMR signal can be seen as well as the donor signal).

When the delay time t_D is very long (cycle rates $< 10^3$ Hz) the spectrum consists only of contributions from pairs with large intrapair separation r , so that broadening due to j - j coupling is very small. The width of the donor magnetic resonance is then about 1.7 mT, as illustrated by the lowest trace in Fig. 7. Following other authors,²⁸ we attribute this residual linewidth to the hyperfine interactions of the donor electron with the nuclei of the host lattice. At the slowest cycle rates, the acceptor line has a residual width of about 2.0 mT and is somewhat asymmetric, possibly as a result of strain broadening.

When the cycle rate is increased, a quite spectacular broadening is observed for both the donor and acceptor lines; see Fig. 7. The broadening corresponds to the increased contributions from shorter-lived pairs, that is pairs of smaller separation r , which have finite j - j coupling interactions and which produce field splittings according to Eqs. (12).

For the donor line, this broadening decreases if (while maintaining constant pulse cycle rate) we rotate the magnetic field to directions ζ well away from the c axis, as would be expected from Eq. (13). However, the broadening does not drop out proportionally to $\cos\theta$ but very much faster. We attribute this anomaly to a breakdown in the optical selection rules as θ increases from zero. Recombination from the sublevels that were nonradiative at $\theta=0$ now becomes less strongly forbidden. For pairs with small intrapair separation, the recombination lifetimes from all four sublevels then can become smaller than the delay time t_D in Fig. 6 and these pairs no longer contribute to the ODMR spectrum. Since these pairs have the larger values of j - j coupling, the ODMR signal narrows. The angular dependence of the linewidth of the acceptor resonance is also anomalous but is in any case more difficult to study because the strain broadening of this line increases rapidly with increasing θ .

The maximum cycle rate in our experiments was ~ 100 kHz (the maximum operating frequency of the lock-in detection). At this pulse rate, the ODMR spectra for B parallel to the c axis have extremely broad wings (see Fig. 7) corresponding to pairs with relatively small values of r . For these pairs, the Coulomb shifts in the emission energy [Eq. (3)] are large. It is now possible to increase the discrimination between pairs of different r (over and above that provided by the time resolution) by restricting the emission wavelengths that are being monitored. This is achieved by interposing a monochromator between the sample and the photomultiplier.

Figure 8 shows examples of ODMR spectra obtained in this way with the monochromator wavelength λ_m set at different points in the high-energy side of the zero-phonon emission band. Here we have placed B parallel to c to eliminate the acceptor resonance (forbidden for this orientation). As the monochromator wavelength λ_m is decreased from 516 nm, the donor resonance signal broadens then splits into two components, as predicted by Eq. (12a). The value of the splitting ΔB increases progressively as λ_m decreases, but the high-field and low-field components remain centered on the isolated-donor g value until the

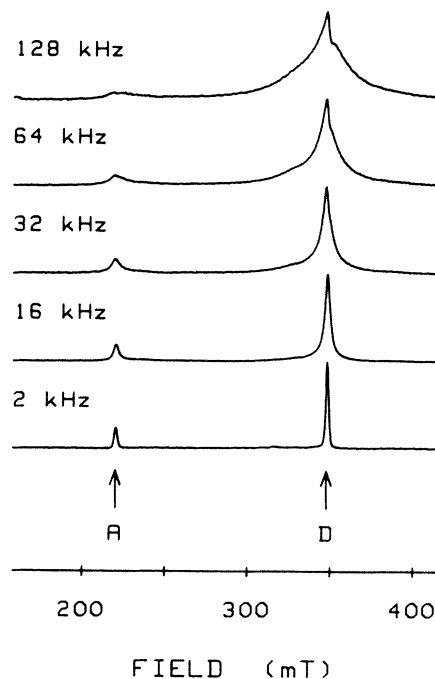


FIG. 7. Time-resolved ODMR spectra obtained by monitoring the whole of the CdS donor-acceptor recombination luminescence, showing the exchange-induced broadening of the donor and acceptor transitions D and A . The vertical axis represents microwave-induced changes of luminescence intensity in arbitrary units: The five spectra shown are normalized to the same peak height. The emission is excited by 488 nm radiation at 2 K; the microwave frequency is 8.7 GHz and the magnetic field is at $\sim 3^\circ$ to the crystal c axis. The pulse sequence is that of Fig. 6 with repetition rate $1/T$ (Hz) as indicated above each spectrum.

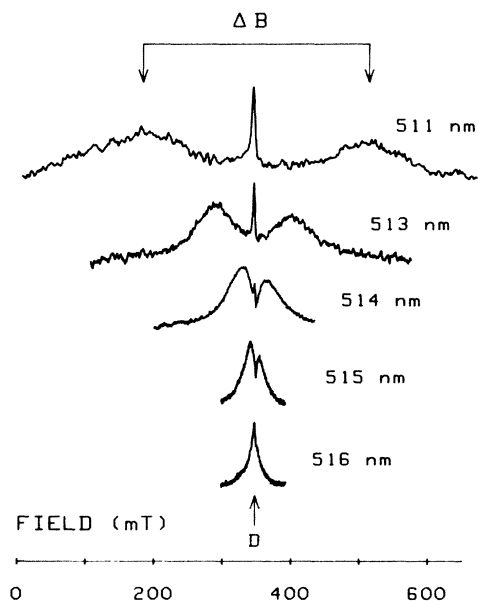


FIG. 8. 8.7 GHz ODMR spectra obtained by monitoring selected wavelengths within the CdS donor-acceptor recombination emission band, showing the exchange-induced splitting of the donor ODMR transition. The arrow labeled *D* marks the resonance field for an isolated donor. The emission is excited by 496 nm radiation at 2 K; the magnetic field is parallel to the *c* axis. The pulse sequence is that of Fig. 6 with $(1/T)=10^5$ Hz. The wavelengths indicated are the monochromator settings.

lower component, which corresponds to the transition $|-1/2, -3/2\rangle \rightarrow |+1/2, -3/2\rangle$ in Fig. 5 reaches zero field. [This component is then replaced by another transition, between $|+1/2, +3/2\rangle$ and $|-1/2, +3/2\rangle$, which moves up in field starting from zero, as can be visualized by imagining the microwave quantum to become progressively smaller in Fig. 5. If the field position of this second transition is given a *negative* sign, Eq. (12a) describes the splitting between it and the high-field transition $|+1/2, +3/2\rangle \rightarrow |-1/2, +3/2\rangle$.]

As can be seen in Fig. 8, the two components become progressively broader as the splitting increases. This is attributed to the finite width of the zero-LO-phonon emission (see Sec. III), so that even with narrow monochromator slit width a range of pair separations r is observed. For a first estimate of the splitting ΔB , we simply measure the positions of the peaks of the two components; a correction procedure is discussed later. As ΔB gets larger, the components become progressively more difficult to observe both because of their increasing width and because the population of pairs of the corresponding spacing gets smaller. Our experiments were limited to values of ΔB just under 1.0 T by noise and baseline fluctuations.

A sharp central signal is also seen in Fig. 8, at the donor resonance position. This signal broadens in turn as the observation wavelength decreases, suggesting that it corresponds to a donor-acceptor system of higher recombination energy. We believe therefore that the line corre-

sponds to centers shallower than those that give the main emission bands, or to an excited state of one of these centers. A high-energy luminescence series, appearing at high cycle rates and shifting with the cycle rate, was observed in the time-resolved emission spectra. (This series is quite distinct from the well-known, free-electron-bound-hole recombination emission.) It gives a shoulder low down on the left of each LO-phonon band of spectrum *a* in Fig. 2. It decays much faster than the main bands so that, in the 10 Hz pulse-rate spectrum, curve *b* of Fig. 2, it appears only as a faint high-energy wing extending out ~ 10 meV from the main zero-LO-phonon band. We believe that the sharp central ODMR signal in Fig. 8 is associated with this higher-energy series. We will not discuss the central ODMR signal further since it does not affect the main results.

The values of ΔB obtained in these field-swept experiments for different settings of λ_m are plotted in Fig. 9. They can, in principle, be related directly to the value of our separation parameter ρ by means of Eq. (3). However, broadening of the two ODMR components, which results, as mentioned above, from the finite width of the optical transitions, is very asymmetric and causes a reduction in the observed value of ΔB . (In fact, at the larger values of λ_m no splitting would be resolved if it were not for the action of the 100-kHz cycle rate in reducing the contribution of the extremely numerous distant pairs.) Large corrections to the measured ΔB are necessary, particularly for the smaller values. This is discussed in Appendix C, where we describe a procedure for obtaining a corrected splitting ΔB for each monochromator setting λ_m . The

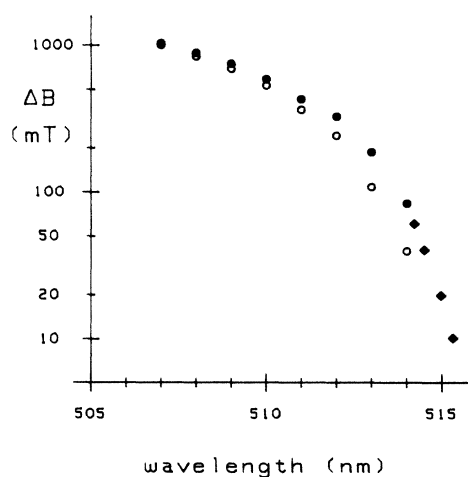


FIG. 9. Measured values of the exchange-induced splitting ΔB of the donor ODMR transition (log scale). Open and solid circles are uncorrected and corrected data, respectively, as obtained by the field-swept method (see text and Fig. 8), plotted as a function of the observation wavelength λ_m . Diamonds represent data obtained by the wavelength-swept method (see text and Fig. 10): the emission-wavelength dependence of the ODMR signal peaks at the wavelength given in the abscissa when the magnetic field is set $\Delta B/2$ away from the center of the donor resonance.

corrected splitting is defined as follows: It is the hypothetical splitting ΔB that would be observed if the emission spectrum from each pair were reduced to a δ function at E_{peak} . The corrections are applied to the data in Fig. 9.

To complement the above measurements, results were obtained by a second method (Fig. 10). Here, the magnetic field was held constant at a particular setting $\Delta B/2$ away from the position of the resonance due to isolated donors. The monochromator was then scanned through the emission spectrum in order to determine the dependence on emission wavelength of those ODMR signals with splitting ΔB . The experiment is not quite as straightforward as this, however, because (as is frequent in ODMR studies of semiconductors) our ODMR spectra are superimposed on a nonresonant background signal, representing microwave-induced changes in luminescence intensity that do not result from magnetic resonance. To correct for this background, a second monochromator scan had to be made for a field setting well away from any resonance. The data recorded during the second scan were then subtracted from those recorded during the first scan to give the correct dependence of the ODMR signal on emission wavelength.

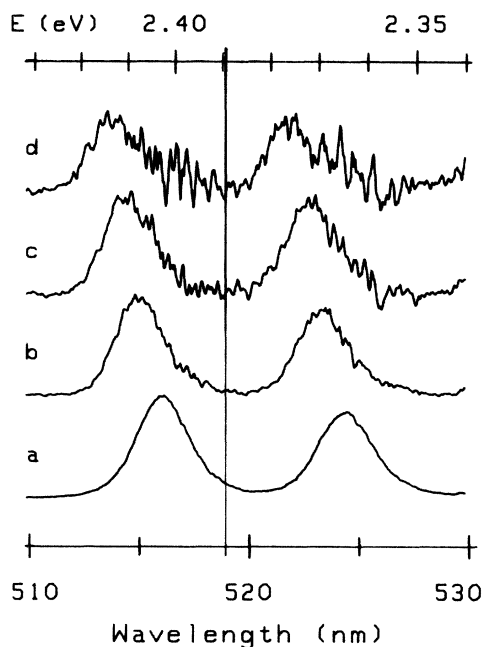


FIG. 10. Emission-wavelength dependences of the donor ODMR signal showing that the signal in the wings of the donor line is associated with shorter emission wavelengths. The magnet is set at the resonance field for isolated donors in trace *a* and at field values $\Delta B/2 = 50, 100,$ and 200 mT away from this field in traces *b, c,* and *d,* respectively. The vertical axis represents ODMR signal intensity (arbitrary units, with gain settings adjusted to make the four traces of comparable height). The wavelength at the peak of the zero-LO-phonon line gives the abscissa and ΔB gives the ordinate for the diamond-shaped data points in Fig. 9. The vertical line marks $E_{\infty, \text{peak}} = 2.389$ eV.

Examples of such emission dependences are shown in Fig. 10 where it is seen that the emission associated with pairs having a given value of exchange splitting ΔB shifts to higher energy as ΔB increases.

The peak of the zero-LO-phonon band in these wavelength-swept spectra gives the value of E_{peak} for pairs having exchange splitting ΔB , without any need for correction, provided that ΔB is large compared with the hyperfine-induced broadening of the ODMR transition (1.7 mT). The minimum value of ΔB that can be studied accurately in this way is therefore about 10 mT. The largest value that can be studied is ~ 50 mT; this is because of signal-to-noise limitations (the number of pairs of

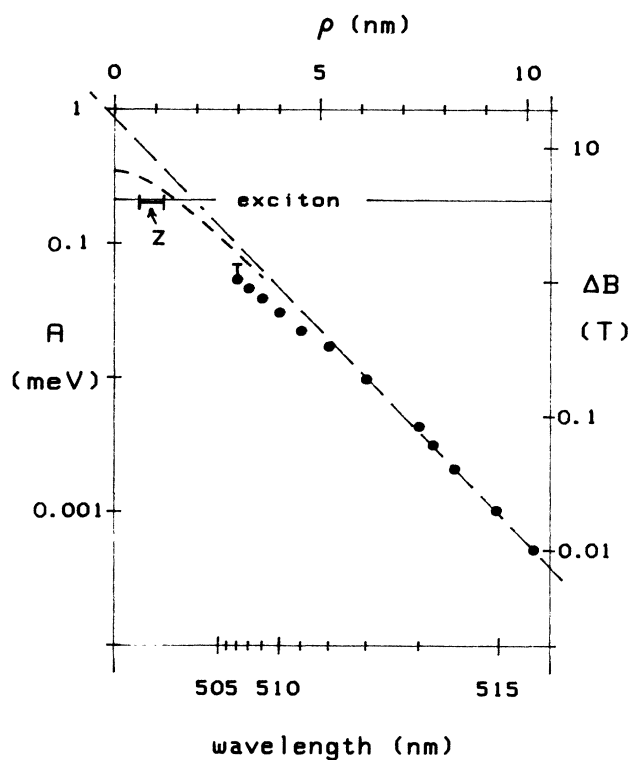


FIG. 11. Logarithmic plot of the electron-hole exchange interaction for a donor-acceptor pair in CdS (scale at left is $\Gamma_6 - \Gamma_5$ splitting in zero-field, scale at right is field splitting of the donor magnetic resonance). The data are that of Fig. 9 but plotted here against a linear scale of donor-acceptor separation distance ρ (only the corrected data are shown; the error bar on the point at 507 nm represents possible error at small ρ due to a nonzero τ_{nr} , see text). The value of ρ for a given donor-acceptor pair was deduced from the peak wavelength of its zero-phonon emission (scale in nm at bottom) as described in the text, with $\epsilon = 8.67$ in Eq. (3). The straight line represents a fit of Eq. (23) to the data points at $\rho = 5 - 10$ nm; its slope corresponds to a value $a_D = 2.75$ nm in Eq. (23). The curve corresponds to the formula [Eq. (24)] of Thuselt and Unger (Ref. 35) with $a_A/a_D = 0.25$, also fitted to the data at $\rho = 5 - 10$ nm. The bar labeled *Z* at $A = 0.20$ meV represents the Zeeman data of Henry *et al.*¹ A horizontal line is drawn at the position representing the free-exciton exchange splitting $A_X = 0.21$ meV.

separation corresponding to ΔB falls off as ΔB increases) and because of increasing difficulty of achieving subtraction of the nonresonant background signal. The results obtained are included in Fig. 9.

In Fig. 11 we plot $\log(\Delta B)$ as a function of the donor-acceptor separation ρ . Here we have translated the wavelengths λ_m of Fig. 9 into a scale of distances ρ using the Coulomb law with $hc(1/\lambda_m - 1/\lambda_{\infty \text{ peak}})$ replacing the quantity $(E - E_{\infty}) = (E_{\text{peak}} - E_{\infty \text{ peak}})$ in Eq. (3). We recall that our estimate of $\lambda_{\infty \text{ peak}}$, based on measurements of radiative recombination rate W , was 518.9 ± 0.1 nm. In Fig. 11 we have used $\lambda_{\infty \text{ peak}} = 518.83$ nm, in the lower part of the error range, for reasons explained in Sec. VI.

As noted earlier, the radiative lifetimes of the pairs observed in these ODMR experiments at 100-kHz cycle rate will be of order 10^{-5} s or smaller. On the other hand, in the time-resolved luminescence studies at 100-kHz to 1-Hz cycle rates, pairs with lifetimes from $\sim 10^{-5}$ up to ~ 1 s were studied. Thus, the distances ρ involved in the ΔB measurements are shorter than those involved in the extrapolation procedure used in Sec. III to determine $\lambda_{\infty \text{ peak}}$. This means that the distance scale in Fig. 11 ought to be fairly *insensitive* to possible error in $\lambda_{\infty \text{ peak}}$. One other aspect of the analysis should be questioned at this point, namely the reliability of the Coulomb law [Eq. (3)] as a means of determining ρ at short distance). Studies of recombining pair systems in other crystals show, however, that the Coulomb term is the dominant distance-dependent term for values of r down to at least a_D . Comparing with data for donor-acceptor pairs in ZnSe,^{29,30} a crystal with properties similar to those of CdS, we estimate that the non-Coulomb terms are only about 3% of the Coulomb energy at the lowest data coordinate in Fig. 11, $\rho = 2.9$ nm. Thus we believe that our distance scale is quite accurate. (More precisely, the horizontal scale in Fig. 11 is a scale of $\epsilon\rho$ and would have to be adjusted if a better estimate of ϵ became available.)

VI. DISCUSSION

In discussing the exchange interaction, the simplest approach (and indeed the only one readily available) is to use a Heitler-London description. The following development follows closely descriptions of exchange in the free exciton given by Elliot³¹ and Fishman.³²

We take the donor-acceptor wave function Ψ to be an

antisymmetrized product of an electronic wave function Ψ_D and a hole wave function Ψ_A :

$$\Psi(\mathbf{r}_1, \mathbf{r}_2) = \mathcal{A}[\Phi_D(\mathbf{r}_1)\Phi_A(\mathbf{r}_2)], \quad (15)$$

where \mathcal{A} is the antisymmetrization operator and $\mathbf{r}_1, \mathbf{r}_2$ are the coordinates of the two particles.

In effective mass theory, $\Psi_D(\mathbf{r}) = \Phi_D(\mathbf{r})u_c(\mathbf{r})$ and $\Psi_A(\mathbf{r}) = \Phi_A(\mathbf{r})u_v(\mathbf{r})$, where Φ_D, Φ_A are normalized envelope functions of appropriate radii centered at the donor and acceptor sites respectively, u_c is a conduction-band electronic wave function at $\mathbf{k} = 0$ and u_v is a valence-band hole wave function at $\mathbf{k} = 0$.

Owing to the antisymmetrization, there will exist an exchange integral of the electron-hole Coulomb interaction of the form

$$\mathcal{E} = \int \Psi_D(\mathbf{r}_1)\Psi_A(\mathbf{r}_2) \frac{e^2}{4\pi\epsilon_0|\mathbf{r}_1 - \mathbf{r}_2|} \times \Psi_D^*(\mathbf{r}_2)\Psi_A^*(\mathbf{r}_1) d^3r_1 d^3r_2. \quad (16)$$

In the absence of spin-orbit coupling and given the three-fold degeneracy of u_v , the 2×6 states of form (15) would group into three degenerate spin singlets and three degenerate spin triplets with separation $\Delta = 2\mathcal{E}$. The effect of (16) could be represented by an equivalent operator (acting on the singlet and triplet spin functions) of form $\mathcal{H} = \Delta/4 - \Delta s_e \cdot s_h$. As mentioned already, however, for shallow pairs in zinc-blende or wurtzite semiconductors where spin-orbit coupling for the hole is much stronger than the exchange interaction, it is more appropriate to use a $j_h = \frac{3}{2}$, $s_e = \frac{1}{2}$ basis in which the effect of (16) is represented by

$$\mathcal{H} = \frac{\mathcal{E}}{2} - \frac{2\mathcal{E}}{3} \mathbf{j}_h \cdot \mathbf{s}_e. \quad (17)$$

Thus, our parameter a in Eqs. (1) and (10) is equivalent to $-2\mathcal{E}/3$. [In the exciton literature, the operator (17) is often written as $\mathcal{H} = \Delta_0 + \Delta_1 \mathbf{J} \cdot \boldsymbol{\sigma}$ with $\Delta_0 = -3\Delta_1/2 = \mathcal{E}/2$ and where $\boldsymbol{\sigma} = 2s_e$ is a Pauli spin operator.]

Using the translational-symmetry properties of the Bloch functions and given that the envelope functions $\Phi_D(\mathbf{r})$ and $\Phi_A(\mathbf{r})$ vary only slowly over the volume Ω of a unit cell, and assuming that the interaction is negligible unless the electron and hole are on the same or nearest-neighbor atoms,^{31,32} one can rewrite Eq. (16) as

$$\mathcal{E} = \frac{1}{\Omega} \int |\Phi_D(\mathbf{r})|^2 |\Phi_A(\mathbf{r})|^2 d^3r \int_{\text{cell}} u_c(\mathbf{r}_1)u_v(\mathbf{r}_2) \frac{e^2}{4\pi\epsilon_0|\mathbf{r}_1 - \mathbf{r}_2|} u_c^*(\mathbf{r}_2)u_v^*(\mathbf{r}_1) d^3r_1 d^3r_2. \quad (18)$$

Note that, as compared to Elliot's treatment of the free exciton,³¹ the only additional level of approximation we have introduced is the assumption that the acceptor envelope function varies only slowly over the volume of the unit cell (the donor envelope function has dimensions similar to those of the exciton envelope function).

Since $u_c(r)$ and $u_v(r)$ are normalized to the unit cell, the second integral in Eq. (18) is of the form $\mathcal{E}_0\Omega^2$, where \mathcal{E}_0 is a constant determined by the band-extrema wave functions. This constant is a molecularlike exchange integral, and is therefore expected to have a magnitude of the order of several electron volts. We can now write Eq.

(18) in the form

$$\mathcal{E} = U\Omega\mathcal{E}_0, \quad (19)$$

where the factor

$$U = \int |\Phi_D(\mathbf{r})|^2 |\Phi_A(\mathbf{r})|^2 dv \quad (20)$$

is the overlap integral of the squares of the envelope functions. The quantity $U\Omega$ in (19) is the probability of finding the electron and the hole in the same unit cell and is a very small number for envelope functions of large radius, even at small intrapair separations. Thus \mathcal{E} is several orders of magnitude smaller than the ‘‘molecular’’ exchange energy \mathcal{E}_0 .

Before proceeding, we note that application of similar arguments to the case of the free exciton^{31,32} gives for the (‘‘short-range’’) exchange integral of the exciton

$$\mathcal{E}_X = |F(0)|^2 \Omega \mathcal{E}_0, \quad (21)$$

where $F(\mathbf{r}_e - \mathbf{r}_h)$ is the function which describes the relative motion of the electron and the hole.

We now examine the way in which the overlap integral U depends on the donor-acceptor separation. In CdS the acceptor radius is small compared with that of the donor [taking the ratio of the averaged effective masses (Appendix A) gives $m_h/m_e \simeq 6$, leading to $a_A/a_D \simeq 0.17$]. The amplitude of the donor envelope function is therefore roughly constant over the region occupied by the hole, so that $|\Phi_D(\mathbf{r})|^2$ can be taken outside the integral in Eq. (20). The quantity U now becomes

$$U = \frac{1}{\pi a_D^3} \exp(-2\rho/a_D), \quad (22)$$

where we have used the hydrogenic form for $\Phi_D(\mathbf{r})$ and where we have used the effective separation ρ as discussed in Appendix A.

The exchange splitting parameter $A = -3a/2 = \mathcal{E}$ should therefore vary as

$$A = A_0 \exp(-2\rho/a_D), \quad (23)$$

where $A_0 = \Omega \mathcal{E}_0 / \pi a_D^3$.

We thus expect a plot of $\log_{10}(A)$ against ρ to be a straight line of slope $-2\log_{10}(e)/a_D$. As shown in Fig. 11, this prediction is satisfied by our data over a large range of values of ρ . The straight line drawn in Fig. 11 gives an excellent fit to the data points in the range 5–9 nm, during which A changes by a factor of about 30. The slope of this line corresponds to $a_D = 2.75$ nm, a value consistent with the value of $a_D = 2.55 \pm 0.3$ nm that we derived from our measurements of radiative recombination rate W , see Sec. III. (We could have fitted the ρ dependence of W with the value $a_D = 2.75$ nm by choosing $\lambda_{\infty \text{ peak}} = 518.83$ nm; thus, to maintain consistency, we have taken $\lambda_{\infty \text{ peak}} = 518.83$ nm in drawing Fig. 11, even though Fig. 11 is fairly insensitive to the exact value of this parameter.)

Of course, Eq. (23) above and Eq. (5) used in Sec. III to deduce a_D (and to give the parameter $\lambda_{\infty \text{ peak}}$ on which our distance scale is based) are not independent: they make the same assumptions about the wave functions.

However, as noted near the end of Sec. V, the range of ρ covered in the two studies is different. It is thus very satisfying to find that the prediction that both A and W should vary as $\exp(-2\rho/a_D)$ gives excellent agreement with our data for values of ρ from about $2a_D$ to about $9a_D$, during which the exponential changes by about 6 orders of magnitude. This is summarized in Fig. 12 which combines Fig. 3 and Fig. 11 (using $\lambda_{\infty \text{ peak}} = 518.83$ nm). It is perhaps one of the best demonstrations ever obtained that the tail of a donor wave function can be represented by a single exponential out to very large distances.

We now consider the situation at small values of ρ . In the limit of vanishingly small ρ , the donor and acceptor core charges cancel and the electron-hole pair transforms into an exciton. Thus we expect a property like the donor-acceptor exchange interaction to tend towards the equivalent property for an exciton as ρ approaches the limit $\rho = 0$.

For the free A exciton, as for the donor-acceptor pair, the Γ_9 hole and the Γ_7 electron couple to give two doublets of symmetry Γ_6 and Γ_5 . These are split by the short-range exchange interaction $\Delta s_e \cdot s_h$ by an amount $A_X = \Delta/2$. A longitudinal-transverse splitting occurs for the Γ_5 doublet giving states Γ_{5T} and Γ_{5L} . According to Fishman and co-workers,^{5,32–34} for a Wannier (i.e., large radius) exciton this does not alter the energy separation between the Γ_{5T} and the Γ_6 levels: the experimentally observable energy difference $E(\Gamma_6 - \Gamma_{5T})$ should thus be al-

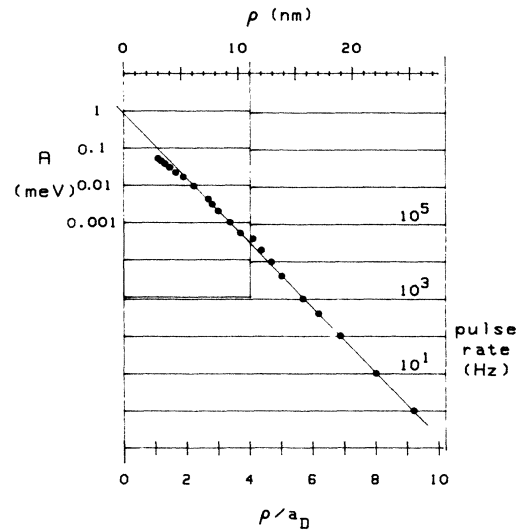


FIG. 12. A composite diagram obtained by overlaying Fig. 11 (redrawn for $\lambda_{\infty \text{ peak}} = 518.83$ nm) onto Fig. 3 and adjusting the vertical positions until the two sets of data match. Donor-acceptor separations are given in nm for $\epsilon = 8.67$ (top scale) and in units of a_D for $a_D = 2.75$ nm (bottom scale). The diagram shows that measurements of exchange interactions A (upper left) and of radiative decay constants W ($\propto 1/T$, where $1/T$ is scale at right) fit a description in which the tail of the donor wave function is represented by a single exponential over six decades of electron density. The straight line is drawn with a slope which corresponds to $a_D = 2.75$ nm if $\epsilon = 8.67$.

most identical with the short-range exchange splitting A_X . This therefore is the appropriate energy to compare with the Γ_6 - Γ_5 splitting for donor-acceptor pairs. The Γ_6 - Γ_5 energy difference for free excitons has been deduced by two different methods, giving 0.23 ± 0.07 meV (Ref. 5) and 0.20 ± 0.03 meV (Ref. 4), respectively. We have therefore taken a value of 0.21 meV for A_X and we have marked this value as a horizontal line drawn across Fig. 11.

Also represented in Fig. 11 is the value of A measured by Henry *et al.* in their optical studies of the strongest resolved emission lines corresponding to donor-acceptor pairs of very small intrapair separation. A subsequent study¹⁰ on CdS crystals doped with lithium isotopes established that the acceptor involved was lithium. Since the common donors in CdS are close to hydrogenic, the data of Henry *et al.*¹ can be compared to our own data on donor-lithium acceptor pairs. Unfortunately, Henry *et al.* could not determine the pair separations involved in their spectrum (because it is extremely difficult to assign pair lines to definite shells of sites in a noncubic crystal). Application of the Coulomb law [Eq. (3)] with our estimate of $E_\infty = 2.393$ eV (not $E_{\infty \text{ peak}}$) gives 1.3–1.5 nm but very large non-Coulomb terms will exist at such short distances. Henry *et al.* suggested that the true distances were about 1.0 nm. By making a comparison with the more recent data on non-Coulomb terms for donor-acceptor pairs in ZnSe,^{29,30} we estimate an upper limit of 1.2 nm for the value of ρ for the pairs of Henry *et al.*, but we can set no obvious lower limit. We represent the data of Henry *et al.* by a horizontal error bar ranging from $\rho = 1.2$ nm down to a somewhat arbitrary lower limit of 0.6 nm (the distance from the Cd site to the second main shell of Cd neighbors). Note that the value of $A = 0.2$ meV obtained by Henry *et al.* is virtually the same as the estimated free-exciton limit.

The straight line which passes through our data points for large ρ extrapolates to a value $A_0 = 0.85$ meV, which is much greater than the free-exciton value. Thus, it is clear that the exponential dependence [Eq. (23)] must break down as ρ decreases. Our experimental data at the smaller values of ρ are indeed beginning to break away from the straight line (see Fig. 11). It is also clear that the data point of Henry *et al.* lies very far below this line.

In fact, our upper data points in Fig. 11 appear to be curving downwards too quickly to extrapolate to the point of Henry *et al.* and to the value of A_X at $\rho = 0$. Unfortunately, our data are less reliable in this interesting region, since the values of ΔB at small ρ may need additional upwards correction. The reason for this is that the "nonradiative" lifetimes τ_{nr} (lifetime of the states with parallel effective spins in Figs. 4 and 5) may become smaller than t_d (the delay time to observation in Fig. 6) for the pairs with small ρ , in which case these pairs would no longer be detected efficiently. Nevertheless (see Appendix C), this effect can explain only part of the deviation of our points from the straight line in Fig. 11. We therefore conclude that the deviation is not a consequence of incorrect analysis of the experimental spectra but that it is real.

We first investigate whether the breakdown of the simple exponential law [Eq. (22)] corresponds to the approxi-

mation we made in replacing the overlap integral of Eq. (20) by a single exponential involving only a_D , an approximation which neglects entirely the spatial extent of the acceptor wave function. The integral of Eq. (20) has an exact analytical form for the case of two *spherical* exponential functions of radii a_D and a_A . This was noted by Thuselt and Unger³⁵ in the only paper that considers improvements to the simple exponential expression for the distance dependence of the donor-acceptor exchange interaction. The expression of Thuselt and Unger (adapted from an equation due to Bindemann³⁶) leads to

$$A = \frac{A_0}{r(\alpha - \beta)^3} \{ e^{-\beta r} [(\alpha^2 - \beta^2)\alpha r - 4\alpha\beta] + e^{-\alpha r} [(\alpha^2 - \beta^2)\beta r - 4\alpha\beta] \}, \quad (24)$$

where $\alpha = 2/a_D$, $\beta = 2/a_A$, and the value of A at $r = 0$ is given by

$$A_0 = \frac{1}{\pi(a_D + a_A)^3} \mathcal{E}_0 \Omega. \quad (25)$$

As already noted by Thuselt and Unger,³⁵ A_0 in (25) is identical to that predicted by effective-mass theory for the exciton, since $|F(0)|^2$ in Eq. (21) is $\pi^{-1}a_X^{-3}$ and the exciton radius $a_X = a_D + a_A$.

Application of Eq. (24) to pairs in CdS is difficult, however, because both wave functions are ellipsoidal. In particular, the hole mass is reported to be very anisotropic, with $m_{||h}$ perhaps several times larger than $m_{\perp h}$ which is about $(0.6 - 0.7)m_0$.³⁷ This is expected to make the acceptor wave function quite anisotropic, and this will make A anisotropic (even in ρ space). To deduce the *maximum* error induced by the exponential approximation, we shall assume a spherical envelope function for the acceptor having radius $a_A = 0.67$ nm, corresponding to the smaller principal value m_h , taken to be $0.68m_0$. Equation (24) (with ρ replacing r) is then fitted to the data points at large ρ where, on the plot of $\log(A)$ against ρ , it gives a straight line. The departure of the Thuselt-Unger formula from the straight line predicted by the simple theory is apparent as ρ decreases (see Fig. 11), but does not become very large until values of ρ of the order of the acceptor radius are reached, much too late for the curve to meet the axis $\rho = 0$ at the exciton value A_X .

We note in passing that the formula of Thuselt and Unger can be fitted rather well to our data at large ρ , to the data of Henry *et al.*¹ at small ρ , and to the exciton value A_X if one assumes a spherical acceptor envelope function with $a_A \simeq 0.4a_D$. However, this seems an unreasonably large value for the acceptor radius, and we therefore consider that allowance for the *finite extent* of the acceptor wave function cannot explain the very strong deviation of A from an exponential law at small ρ . Also, the absence of any marked anisotropy in A noted by Henry *et al.*¹ in their study of pairs having very small ρ implies that the *shape* of the acceptor wave function cannot be having any strong effect on the value of A .

We next note that the data of Fig. 11 could be explained if we assumed that the donor envelope function is

not a simple exponential but consists, for example, of two exponentials, with an effective Bohr radius greater than 2.75 nm at $\rho < 5$ nm transforming to the value $a_D = 2.75$ at $\rho = 5$ nm. Such an unorthodox form for the wave function seems improbable, however, because there is no obvious mechanism that could cause the wave function to drop off more *rapidly* at large distance. Moreover, as noted earlier, the “outer” radius of 2.75 nm is close to the value predicted by effective mass theory, and this is the value one would expect in the inner region $\rho < 5$ nm, which contains most of the electron density.

Thus, we conclude that the strong deviation of the data from a simple exponential law, which is much larger than one would expect on the basis of the Thueselt-Unger formula, results more probably from some failing in the Heitler-London procedure leading to Eqs. (18)–(20) and (24). This procedure, representing the electron-hole wave function by an antisymmetrized product of *unperturbed* donor and acceptor wave functions [Eq. (15)], clearly cannot be correct at small separations. Improved product wave functions, including those in which, for example a_D, a_A are variational parameters, have been developed for calculating the optical transition energy, but unfortunately only for pairs in cubic crystals (GaP, ZnSe),³⁸ not in CdS. In any case, it is not obvious that an improved product wave function would help. As noted earlier, Eq. (24), based on a simple, unperturbed product wave function that must be quite wrong at $r=0$, gives (for reasons that are obscure) a value for $A(r=0)$ that is *identical* to that predicted by the correct effective-mass theory of the exciton. Thus, in Fig. 11, we might equally well have fitted the short-dashed curve to A_X at $\rho=0$, in which case it would have given values of A much too small at large ρ . In other words, since we have no way of estimating \mathcal{E}_0 , we cannot say whether the value of A predicted by a product-wave-function description is most in error at small ρ or at large ρ .

In fact, since the exchange interaction could be very sensitive to the fine details of the wave function in the overlap region, an accurate theory of this interaction will probably need more sophisticated wave functions. For the similar problem of calculating radiative recombination rates, several authors have pointed out the importance of the electron-hole *correlation*. Wave functions that include a fully correlated “exciton-like” component $\Psi(\mathbf{r}_e - \mathbf{r}_h)$ have been proposed for this purpose³⁹ but, again, only cubic crystals have been treated. Thus, in conclusion, we emphasize that further development of this kind of theory, including treatment of the effects of crystal anisotropy, would be very useful for understanding the detailed behavior of the distance dependence of the donor-acceptor exchange interaction.

VII. CONCLUSIONS

The results described in this paper give the first experimental determination of the way in which the electron-hole exchange interaction for a donor-acceptor pair varies with the intrapair separation. For effective separations ρ between $\sim 2a_D$ and $\sim 4a_D$, the exchange splitting A is found to vary according to $A_0 \exp(-2\rho/a_D)$, with

$a_D = 2.75$ nm. This value of a_D is consistent with the value $a_D = 2.55 \pm 0.3$ nm that fits the ρ dependence of the radiative decay constant W as determined from the time-resolved luminescence spectroscopy of pairs with values of ρ between $\sim 5a_D$ and $\sim 9a_D$. Thus the assumption of a simple hydrogenic envelope wave function for the donors is found to be valid for values of ρ from $2a_D$ to $9a_D$, a range in which the probability function decays by 6 orders of magnitude (Fig. 12). We believe this to be the most accurate determination of the behavior of a donor envelope function yet obtained for distances greater than the Bohr radius. It should be noted also that the values for a_D obtained in this work are close to the value of 2.39 nm predicted by effective mass theory.

The value of $A_0 = 0.85$ meV obtained by extrapolating the exponential expression to zero separation is much greater than the experimentally determined value $A_X (= 0.21$ meV) for the exchange interaction in the free exciton.^{4,5} Since the trapped electron-hole pair must transform to an exciton as $\rho \rightarrow 0$, this implies that the exponential formula for A must break down at small separations. Such a breakdown is predicted by the formula of Thueselt and Unger,³⁵ but Fig. 11 shows that it occurs at values of ρ that are larger than expected. The currently available theories do not appear to account *simultaneously* for the value of A_X and for the values of the exchange splitting measured for donor-acceptor pairs in the present investigation. Our results therefore point to the need for improved theories for the exchange interaction between a donor and an acceptor separated by a distance r , and in particular at values of r so small that the electron-hole pair begins to approximate to an exciton. It is hoped that the present data will provide a stimulus for the development of such theories.

ACKNOWLEDGMENTS

We are grateful to G. Fishman of Laboratoire de Spectrométrie Physique, Grenoble and to A. G. Hall of Hull University for helpful discussions concerning theoretical aspects of this work. We also thank J. E. Nicholls of Hull University for supplying the CdS crystal. One of us (J.J.D.) wishes to thank the Royal Society for financial support during one of several visits to Grenoble and the University of Hull for granting a leave of absence.

APPENDIX A: EFFECTS OF CRYSTAL ANISOTROPY

It can be seen from Eq. (2) that there is not a unique correspondence between the zero-phonon energy $h\nu$ and the true intrapair separation r : the correspondence is in fact between $h\nu$ and the quantity

$$\epsilon_{\rho r} = (\epsilon_1 \epsilon_{\parallel} \sin^2 \theta + \epsilon_1^2 \cos^2 \theta)^{1/2} r,$$

so that a given emission wavelength can correspond to a range of values of r according to the different values of θ . We now show that this need not have any serious consequences in our work.

When considering a crystal of hexagonal symmetry, several authors have made use of a coordinate transformation that renders the Coulomb interaction isotropic, e.g.^{18,37} If the donor-acceptor separation in real space is

defined by coordinates x, y, z (with z axis along the c axis), new coordinates $X, Y,$ and Z are defined such that $X=x,$ $Y=y,$ and $Z=(\epsilon_{\perp}/\epsilon_{\parallel})^{1/2}z$. The Coulomb term in Eq. (2) now becomes $e^2/(4\pi\epsilon\epsilon_0\rho)$, where $\epsilon=(\epsilon_{\perp}\epsilon_{\parallel})^{1/2}$ and $\rho^2=X^2+Y^2+Z^2$. There is thus a unique correspondence between the emission wavelength λ and the new coordinate ρ [at least for the range of distances where Eq. (2) is valid].

To proceed further, we need to examine the wave function of a donor electron in an anisotropic medium. The time-independent Schrödinger equation for the donor has the form

$$\left[-\frac{\hbar^2}{2m_{\perp}} \left(\frac{\partial^2}{\partial x^2} + \frac{\partial^2}{\partial y^2} \right) - \frac{\hbar^2}{2m_{\parallel}} \frac{\partial^2}{\partial z^2} - \frac{e^2}{4\pi\epsilon_{\theta}\epsilon_0 r} \right] \psi = E\psi,$$

where ϵ_{θ} is anisotropic and where m_{\parallel} and m_{\perp} refer to the electron. In the new coordinate scheme, the equation becomes

$$\left[-\frac{\hbar^2}{2m} \nabla^2 - \frac{e^2}{4\pi\epsilon\epsilon_0\rho} + \eta\mathcal{H}' \right] \psi = E\psi, \quad (\text{A1})$$

where

$$\epsilon = (\epsilon_{\perp}\epsilon_{\parallel})^{1/2}, \quad \frac{1}{m} = \frac{2}{3m_{\perp}} + \frac{\epsilon_{\perp}}{3m_{\parallel}\epsilon_{\parallel}}, \quad (\text{A2})$$

$$\mathcal{H}' = -\frac{\hbar^2}{2m} \left[\frac{1}{2} \left(\frac{\partial^2}{\partial X^2} + \frac{\partial^2}{\partial Y^2} \right) - \frac{\partial^2}{\partial Z^2} \right], \quad (\text{A3})$$

and

$$\eta = \frac{m_{\parallel}\epsilon_{\parallel} - m_{\perp}\epsilon_{\perp}}{m_{\parallel}\epsilon_{\parallel} + \frac{1}{2}m_{\perp}\epsilon_{\perp}}. \quad (\text{A4})$$

If $\eta=0$, Eq. (A1) represents a hydrogenic problem, for which the ground-state envelope wave function has the form

$$(\pi a_D^3)^{-1/2} \exp(-\rho/a_D),$$

where

$$a_D = 4\pi\epsilon\epsilon_0\hbar^2/me^2.$$

From magneto-optical studies of the excited states of shallow chlorine donors in CdS, Henry and Nassau⁴⁰ found values of $m_{e\parallel}=0.180m_0$ and $m_{e\perp}=0.190m_0$ for donor electrons. The measured low-temperature values¹⁹ of $(\epsilon_{\parallel}, \epsilon_{\perp})$ are, from infrared reflectivity¹⁸ (8.92, 8.42), from Raman spectroscopy (9.12, 8.45) (Ref. 41), and from electrical measurements (9.53, 9.02) (Ref. 42) and (9.00, 8.37) (Ref. 43). The anisotropy in ϵ_{θ} is therefore in the opposite sense to that of the effective mass, so that the parameter η is small, being less than 0.1. For example, Henry and Nassau⁴⁰ found that the quantity α , defined as $1-(m_{\perp}\epsilon_{\perp}/m_{\parallel}\epsilon_{\parallel})$, is equal to 0.050 ± 0.005 , so that $\eta=0.033$. The operator $\eta\mathcal{H}'$ may therefore be regarded as a very weak perturbation. We conclude that a radial dependence of the form $\exp(-\rho/a_D)$ is a good representation of the donor envelope function, which is therefore of spherical symmetry in ρ space. This conclusion is also justified by our experimental results.

As discussed in the text, the use of a donor envelope function of this form leads, for large intrapair separations, to recombination rates and exchange splittings of the form $W=W_0\exp(-2\rho/a_D)$ and $A=A_0\exp(-2\rho/a_D)$, respectively. There is thus a one-to-one correspondence between A (or W) and ρ , and hence between A (or W) and the optical emission energy, even in the presence of an anisotropic dielectric constant.

The effective mass m_e for electrons used in the text is found from Eqs. (A2) and the data of Henry and Nassau⁴⁰ to be $m_e=0.192m_0$. The corresponding value for holes is found to be $m_h=1.2m_0$, where we have used $m_{h\parallel}=5.0m_0$ and $m_{h\perp}=0.68m_0$.³⁷ Because the effective mass for holes is very anisotropic, the factor η is large in Eq. (A1) if it is applied to the case of the acceptor, and the acceptor envelope function cannot then be expected to be spherical in ρ space.

APPENDIX B: FURTHER ANALYSIS OF THE TIME-RESOLVED LUMINESCENCE

The purpose of the time-resolved luminescence spectroscopy (Sec. III) was twofold. First, to establish a value of E_{∞} and, second, to estimate a_D . In this appendix, we give an approximate theory of the form of the emission spectrum to be obtained for the pulsed-detection scheme of Fig. 1, taking into account the finite width of the zero-LO-phonon line and allowing for the effect of the distribution of pair separations. We approximate the pulse sequence of Fig. 1 by an idealized sequence with a very narrow laser pulse of width δ at time $t=0$ and very narrow detection gates at $t_1 \simeq 0.5T$ and $t_2 \simeq T$, where T is the repetition period.

We consider pairs of separation ρ and recombination rate constant $W(=1/\tau)$. Suppose that at the end of the laser pulse the intensity from such pairs is I_0 . The detected signal is the difference between the luminescence intensities at t_1 and t_2 :

$$\mathcal{S} = I_0(e^{-0.5WT} - e^{-WT}). \quad (\text{B1})$$

During each laser pulse the luminescence intensity is restored to its original value I_0 . Now $I_0 \propto Wn^*(\delta)$ where $n^*(\delta)$ is the number of pairs excited at the end of the laser pulse ($t=\delta$). For low laser power (unsaturated case)

$$n^*(\delta) = c\delta + n^*(0), \quad (\text{B2})$$

where c is the excitation rate (number of excited states created per unit time) and $n^*(0)$ is the number already excited just before the laser pulse. (It is the latter term whose importance has been emphasized by Dunstan and coworkers.^{20,21} This is the background concentration built up by the repetition of the pulse sequence.) Writing $n^*(0) = n^*(\delta)e^{-WT}$, we deduce

$$n^*(\delta) = c\delta/(1 - e^{-WT}). \quad (\text{B3})$$

With δ a fixed fraction of T (independent of the cycle rate), i.e., $\delta = fT$, we have $I_0 \propto cfTW/(1 - e^{-WT})$. Combination with Eq. (B1) gives

$$\mathcal{S}(\rho) \propto c(\rho)ye^{-y}/(1 + e^{-y}), \quad (\text{B4})$$

where we have substituted $y = 0.5WT$. We shall assume the simplest possible expression for the excitation rate $c(\rho)$, namely that it is of the form $kn(\rho)$, where k is a constant depending on the laser power [although a form $c(\rho) \propto n^2(\rho)$ is also plausible, see below].

In the above, we assume a very low relative concentration of excited pairs (no saturation) which ought to be appropriate to our experiments where we excited below the band gap and where we reduced the laser power by 1000 on going from 100 kHz to 1 Hz pulse rate. On the other hand, if laser power high enough to saturate all pairs were used, then $n^*(\rho) = n(\rho)$ and the signal would be

$$[\mathcal{S}(\rho)]_{\text{sat}} \propto n(\rho)(1/T)ye^{-y}(1-e^{-y}). \quad (\text{B5})$$

Compared to Eq. (B4), this gives a response function weighted towards somewhat shorter lifetimes.

To calculate the spectrum, we integrate $\mathcal{S}(\rho)$ in (B4) or (B5) over all values of ρ for various settings λ of the monochromator. In this calculation, we assume $W = W_0 \exp(-2\rho/a_D)$, where W_0 and a_D are parameters to be adjusted to fit experiment (the simple exponential law ought to be valid for the large distances involved in the luminescence study). We take a very simple form for $n(\rho)$, namely $n(\rho) \propto 4\pi\rho^2$. This is the correct statistical form at small ρ (the true distribution of course flattens at some $\rho \sim \rho_{\text{mean}} \sim 1/N^{1/3}$, but it is only at small ρ that the shape of the population distribution has any marked effect). Finally, to allow for the finite width of the zero-LO-phonon line (the TO-phonon broadening of Moroz *et al.*¹⁰), we approximate the shape of the line by a Gaussian curve \mathcal{G} of full width at half height $\Delta E = 0.010$ eV. We take the origin of energy at $E_{\infty \text{ peak}}$ so that the Gaussian curve $\mathcal{G}(E, \rho)$ for pairs of separation ρ is centered at $e^2/4\pi\epsilon\epsilon_0\rho$.

With the monochromator set at $E_m (=hc/\lambda_m)$, the detected signal is

$$\mathcal{S}(E_m) = \int_0^{\infty} \mathcal{S}(\rho)\mathcal{G}(E_m, \rho)d\rho. \quad (\text{B6})$$

Equation (B6) was integrated numerically for a range of values of E_m to give the shape of the emission band. The procedure was repeated for various values of T and the peak energies ($E_{\text{peak}} - E_{\infty \text{ peak}}$) of the calculated bands were extracted. The results of this calculation, when plotted as a graph of $\log(1/T)$ against $(E_{\text{peak}} - E_{\infty \text{ peak}})^{-1}$, gave a straight line at large values of ρ . Therefore, the theoretically calculated graph was fitted to the measured values of $(E_{\text{peak}} - E_{\infty \text{ peak}})^{-1}$ from our time-resolved spectra at low cycle rates (with $E_{\infty \text{ peak}}$ chosen to make the data points lie on a straight line). The fitted curve for the case of no optical saturation is shown in Fig. 3 and corresponds to a value of $W_0 = 2.0 \times 10^8 \text{ s}^{-1}$.

The calculated graphs curve upwards at small ρ on the $\log(1/T)$ plot, essentially because there are very few pairs with small ρ . However, it is seen from Fig. 3 that the deviation of the data points from a straight line begins to become significant at lower cycle rates than expected from our theory.

The theoretical graph can be made to curve upwards at lower cycle rates by assuming that the creation rate $c(\rho)$ in Eq. (B4) is proportional to $n^2(\rho)$: this might be a more

appropriate form for $c(\rho)$ since, even for the present case of below band gap excitation, creation of a hole at the acceptor and of an electron at the donor could be uncorrelated events. The resulting graph (not shown in Fig. 3) has more curvature in the region of the upper data points, but this curvature is still insufficient to fit the points.

We believe that the anomalous deviation of our data from a straight line plot is, in fact, due to the effect of the donor-acceptor exchange interaction. The deviation begins to become apparent at values of ρ of about $4a_D$ to $5a_D$, and at this separation the exchange splitting is about 10^{-7} eV (see Fig. 12) and is becoming greater than the hyperfine interactions between the donor electron and the Cd nuclei.²⁸ For larger ρ values, the Γ_5 doublet (radiative) and Γ_6 doublet (nonradiative) would be mixed by the hyperfine interactions, averaging W_r and W_{nr} (see notation of Appendix C) to give a value $(W_r + W_{nr})/2 \simeq W_r/2$ for each of the four states. The vertical position of the straight line that fits the data for large ρ would then correspond to a rate constant of $W_r/2$. For ρ smaller than about $4a_D$, the exchange interaction becomes sufficiently strong to produce well-defined Γ_5 and Γ_6 states. The time-resolved luminescence experiment would then measure a rate constant which tended towards W_r and the points would be expected to deviate upwards as is indeed observed in Fig. 3. The graph should eventually run parallel to the calculated curve in Fig. 3 but at a distance $\log_{10}(2)$ higher; however, such behavior lies beyond the range of our measurements.

APPENDIX C: CORRECTIONS TO THE ODMR DATA

In the ODMR experiments described in Sec. V, a monochromator was used to select a narrow range of intrapair separations. However, the resolution obtained in this way is limited by the width $\Delta \sim 0.01$ eV of the zero-phonon emission of a donor-acceptor pair in CdS. In this Appendix, we examine the effect of the optical line broadening on the shape of the wavelength selected field-swept ODMR spectra.

As in Appendix B, we take the zero of energy at $E_{\infty \text{ peak}}$, so that the optical emission band from pairs of separation ρ peaks at $E_{\text{peak}} = e^2/(4\pi\epsilon\epsilon_0\rho)$. In the present analysis, to get a good simulation of the ODMR line shape, we have found it necessary to use the true, asymmetric shape $\mathcal{B}(E - E_{\text{peak}})$ of the optical band instead of the Gaussian form $\mathcal{G}(E - E_{\text{peak}})$ used in Appendix B. Then with the monochromator set to energy E_m , pairs in a range of separations $d\rho$ at ρ will give an ODMR signal intensity

$$\mathcal{S}(\rho)d\rho = \mathcal{R}(\rho)\mathcal{B}(E_m - E_{\text{peak}})d\rho, \quad (\text{C1})$$

where $\mathcal{R}(\rho)$ is the ODMR response function (see below).

In the field-swept ODMR spectrum, these pairs will give a pair of lines at field displaced from the isolated-donor signal by $\pm A/g_{\parallel}^D\beta$, where A is the exchange interaction for this value of ρ . Then if we assume (at least initially) that $A \propto \exp(-2\rho/a_D)$, the shape of the field-swept ODMR spectrum is given by

$$\mathcal{O}(A)dA \propto \mathcal{R}(\rho)\mathcal{B}(E_m - E_{\text{peak}})(1/A)dA \quad (\text{C2})$$

where $\mathcal{O}(A)dA$ is the total ODMR signal in a range dA at A .

If the width ΔE of the optical emission profile were reduced to zero, the ODMR spectrum would consist of two sharp lines separated in field by $\Delta B = 2A/g_{\parallel}^D\beta$ (for the donor resonance with B parallel to the c axis) and it would be possible to obtain the relation between A and ρ directly. Because $\Delta E \neq 0$, the lines are broadened and skewed towards smaller splittings. From Eq. (C2), however, we can estimate the extent of these effects.

To obtain the ODMR response function \mathcal{R} , we shall assume that the pairs in states $|\pm\frac{1}{2}, \mp\frac{3}{2}\rangle$ in Fig. 4 radiate strongly with a decay constant

$$W_r (= \tau_r^{-1}) = W_r(0)\exp(-2\rho/a_D)$$

and that those in states $|\pm\frac{1}{2}, \pm\frac{3}{2}\rangle$ have a decay constant

$$W_{nr} (= \tau_{nr}^{-1}) = W_{nr}(0)\exp(-2\rho/a_D),$$

where $W_{nr}(0) \ll W_r(0)$. We can thus write $W_{nr} = W_r/v$, where v is a number independent of ρ .

In order to make calculation of the response function tractable, approximations have to be made that depend on the values of W_r or W_{nr} relative to the repetition frequency ($1/T$) of the pulse sequence. We shall consider two separate conditions, appropriate to large and small values of ρ , respectively, namely (a) $W_{nr}T \ll 1$ with $W_rT \sim 1$ or greater and (b) $W_rT \gg 1$ (with no condition on $W_{nr}T$).

Under the first condition, $W_{nr}T \ll 1$, the number of pairs n_{nr}^* in nonradiative states does not change significantly during the cycle. When microwave power is applied at resonance, pairs are transferred from the nonradiative states to the radiative states at a rate proportional to the current value of n_{nr}^* . (With $W_{nr} \ll W_r$, then $n_{nr}^* \gg n_r^*$ and the value of n_r^* is immaterial; we are assuming here that the microwave power available, 10 W into a cavity having $Q \sim 3000$ and with signal-enhancing field modulation applied, is too low to saturate the microwave transition.) The number of pairs transferred is taken to be proportional to the microwave power μ , to n_{nr}^* and to the duration θ of the microwave pulse. The transferred pairs now radiate (with decay constant W_r) and contribute an additional amount to the luminescence. Determining the difference in light output between the alternate detector gate periods in Fig. 6 (and neglecting the effects of a microwave pulse in one cycle on the light output in later cycles, which effects are small provided $W_rT \sim 1$ or greater), we find that the ODMR signal from pairs of given ρ is proportional to

$$\mathcal{R}(\rho) = \mu n_{nr}^* \theta \left[1 - \frac{1 - e^{-x}}{x} \right] \quad (\text{C3})$$

where $x = W_r\theta$, with $\theta = 10^{-6}$ s in our experiments.

If $W_{nr}T \ll 1$, the number of nonradiative pairs that decay in one cycle is simply the number that are transferred to radiative states per cycle, namely $\mu n_{nr}^* \theta$. This number must equal the number of pairs excited to nonradiative states by the laser per cycle. Thus we can replace $\mu n_{nr}^* \theta$ in (C3) by a factor proportional to the creation rate $c_{nr}(\rho)$ where (cf. Appendix B) we take this rate to be proportional to $n(\rho)$.

Substituting the response function (C3) into Eq. (C2), we have calculated the expected shapes of the ODMR spectra for the different values of the monochromator energy E_m used in the experiments. The optical band shape $\mathcal{B}(E - E_{\text{peak}})$ was taken from a time-resolved luminescence spectrum at long delay time (curve *b* of Fig. 2). We have also calculated the corresponding ODMR spectra for the hypothetical case of a very narrow optical line (centered at E_{peak}). Comparison of the two cases gives the correction factor defined in Sec. V, that is the factor by which we multiply the apparent field splitting (measured between the two ODMR peaks) to get the true value of ΔB for pairs having $E_{\text{peak}} = E_m$.

To begin these calculations, we injected the value of $a_D = 2.55$ nm given by the time-resolved luminescence study. As noted in Sec. VI, the resultant corrected values of ΔB fit $a_D = 2.75$ nm (at $\rho > 5$ nm). Therefore, the correction procedure was recycled using the latter value, but this made only marginal changes on the logarithmic scale of Fig. 11. For the larger values of E_m (smaller values of λ_m) the results are not very sensitive to the exact value of the parameter $W_r(0)$. For $\lambda_m > 514$ nm, however, the corrections become very large (exceeding a factor of 2) and unduly sensitive to the large uncertainty in $W_r(0)$. Therefore, we have retained only the results for $\lambda_m \leq 514$ nm from the data obtained by the field-swept method. For $\lambda_m > 514$ nm, reliable data is available from the wavelength-swept method (see Sec. V). The correction procedure outlined above raises the values of ΔB measured by the field-swept method, making them consistent with those obtained by the wavelength-swept method, see Fig. 9. We took $W_r(0) = 3 \times 10^8 \text{ s}^{-1}$, which gave the best match between the two sets of data. This value is comparable to the value $W_r(0) \approx 2W_0 = 4 \times 10^8 \text{ s}^{-1}$, where W_0 is the rate constant measured in the time-resolved luminescence experiments at large ρ where W_r and W_{nr} are averaged (see the discussion at the end of Appendix B); the difference lies within the sum of the very large experimental errors associated with the two estimates of $W_r(0)$.

Confidence in the procedure used here is enhanced by the fact that our simulated spectra reproduce reasonably well the large ODMR linewidths observed experimentally, which increase in absolute value as the field splitting ΔB gets larger (see Fig. 8). We have further checked the correction procedure by introducing an artificial optical line broadening in the experiment by opening the monochromator slits. This is observed to decrease the field-separation between the peaks in the ODMR spectrum in a manner consistent with that predicted by the correction procedure.

The correction factors calculated by the above procedure are used in Figs. 9 and 11. For the smaller separations, the validity of the assumption that $W_{nr}T \ll 1$ needs to be checked. With $W_r(0) = 3 \times 10^8 \text{ s}^{-1}$, the value of W_rT is ~ 1 at $\rho = 4a_D$, increasing to ~ 50 at $\rho = 2a_D$. For $W_{nr}T$ to be $\ll 1$ over this range would require that the ratio $v = W_r/W_{nr}$ be greater than 100, which is not unreasonable. If v were much smaller than this, the correction factor based on Eq. (C3) could be inaccurate at $\rho \sim 2a_D$, but by then the calculated correction has become

very small.

For the closest pairs ($\rho \sim 1.5a_D$), the condition $W_{nr}t_d \ll 1$ is quite likely not satisfied, that is, not only the radiative states but also the nonradiative states may decay substantially during the delay time $t_d \sim 10^{-6}$ s between the end of the laser pulse and the opening of the detector gate (see Fig. 6). However, the radiative rate constant is now such that $W_r T \gg 1$. This is condition (b) mentioned earlier in this Appendix. It is now possible to obtain a different ODMR response function (with no restriction on $W_{nr}T$ or on $W_{nr}t_d$) of the form

$$\mathcal{R}(\rho) = \mu c(\rho) \delta \theta \left(\frac{e^{-W_{nr}t_d}(1 - e^{-W_{nr}\theta})}{1 - e^{-W_{nr}T}} \right), \quad (C4)$$

where δ is the laser pulse width.

We have considered the effect of the response function (C4) for the monochromator set at 507 nm, that is for the data point at the smallest value of ρ in Figs. 9 and 11, for various values of $v = W_r/W_{nr}$. We find that with values of $v > 5$, the maximum correction factor to be applied to the observed ΔB at 507 nm is 1.3. This is indicated by an error bar in Fig. 11. A correction of this kind, compensating for the fact that the cycle rate of the ODMR experiment could be too slow for efficient detection of pairs with very small ρ , would improve the consistency of our data with the data point of Henry *et al.* and with the free exciton value (see Fig. 11). However, to raise our data points for small ρ by more than the amount indicated by the error bar in Fig. 11 would require unreasonably small values of v , and we therefore conclude that the deviation of the exchange splitting from the straight line and from the Thuselt-Unger formula in Fig. 11 is real.

*Permanent address: Department of Physics, University of Hull, Hull HU6 7RX, England, United Kingdom.

¹C. H. Henry, R. A. Faulkner, and K. Nassau, *Phys. Rev.* **183**, 798 (1969).

²D. C. Reynolds and T. C. Collins, *Phys. Rev.* **188**, 1267 (1969).

³For recent reviews of the ODMR technique in semiconductors, see, e.g., B. C. Cavenett, *Adv. Phys.* **30**, 475 (1981); J. J. Davies, *Proceedings of the Second International Conference on II-VI Compounds, Aussois, 1985* [*J. Cryst. Growth* **72**, 317 (1985)].

⁴I. Broser and M. Rosenzweig, *Solid State Commun.* **36**, 1027 (1980); *Phys. Rev. B* **22**, 2000 (1980).

⁵N. T. Thang and G. Fishman, *Phys. Rev. B* **31**, 2404 (1985).

⁶R. T. Cox, J. J. Davies, and R. Picard, in *Proceedings of the 17th International Conference on the Physics of Semiconductors, San Francisco, 1984*, edited by J. D. Chadi and W. A. Harrison (Springer-Verlag, New York, 1985), p. 651.

⁷F. A. Kröger, *Physica* **7**, 1 (1940); C. C. Klick, *J. Opt. Soc. Am.* **41**, 816 (1951); L. S. Pedrotti and D. C. Reynolds, *Phys. Rev.* **120**, 1664 (1960).

⁸K. Colbow, *Phys. Rev.* **141**, 742 (1966).

⁹D. G. Thomas, R. Dingle, and J. D. Cuthbert, in *Proceedings of the International Conference on II-VI Semiconducting Compounds, Brown University, 1967*, edited by D. G. Thomas (Benjamin, New York, 1967), p. 863.

¹⁰C. H. Henry, K. Nassau, and J. W. Shiever, *Phys. Rev. Lett.* **24**, 820 (1970); *Phys. Rev. B* **4**, 2453 (1971).

¹¹J. L. Patel, J. E. Nicholls, and J. J. Davies, *J. Phys. C* **14**, 1339 (1981).

¹²M. Moroz, Y. Brada, and A. Honig, *Solid State Commun.* **47**, 115 (1983).

¹³I. Broser, J. Gutowski, and R. Riedel, *Solid State Commun.* **49**, 445 (1984).

¹⁴I. Broser, D. Pätke, and M. Rosenzweig, *Solid State Commun.* **54**, 849 (1985).

¹⁵See, e.g., P. J. Dean, in *Progress in Solid State Chemistry*, edited by J. D. McCaldin and G. Somorjai (Pergamon, Oxford, 1973), Vol. 8, p. 1.

¹⁶This formula, frequently cited in the literature (e.g., Refs. 1, 15, 18, 26, 37, and 40) can be derived by assuming that the potential due to a point charge q is of the form

$$q / \{ 4\pi\epsilon_0 [b(x^2 + y^2) + cz^2]^{1/2} \},$$

where z is along the c axis. The requirement that $\text{div} \mathbf{D} = 0$ gives $b = \epsilon_{||}c/\epsilon_{\perp}$. By application of the theorem of Gauss to a cylindrical surface surrounding q , it is readily shown that $c = \epsilon_{\perp}^2$.

¹⁷R. F. Brunwin, B. C. Cavenett, J. J. Davies, and J. E. Nicholls, *Solid State Commun.* **18**, 1283 (1976).

¹⁸J. Flohrer, E. Jahne, and M. Porsch, *Phys. Status Solidi B* **91**, 467 (1979). These authors summarize values of $\epsilon_{||}$ and ϵ_{\perp} obtained by a variety of methods.

¹⁹H. W. Verleur and A. S. Barker, *Phys. Rev.* **155**, 750 (1967).

²⁰D. J. Dunstan, *Philos. Mag. B* **46**, 579 (1982).

²¹D. J. Dunstan, S. P. Depinna, and B. C. Cavenett, *J. Phys. C* **15**, L425 (1982); S. P. Depinna and D. J. Dunstan, *Philos. Mag. B* **50**, 579 (1984); D. J. Dunstan, *ibid.* **52**, 111 (1985).

²²D. G. Thomas, J. J. Hopfield, and W. M. Augustyniak, *Phys. Rev.* **140**, A202 (1965).

²³K. Morigaki, *J. Phys. Soc. Jpn.* **19**, 1253 (1964).

²⁴D. G. Thomas and J. J. Hopfield, *Phys. Rev.* **128**, 2135 (1962).

²⁵J. J. Davies and J. E. Nicholls, *J. Phys. C* **15**, 5321 (1982).

²⁶J. J. Davies, R. T. Cox, and J. E. Nicholls, *Phys. Rev. B* **30**, 4516 (1984).

²⁷D. Block, A. Hervé, and R. T. Cox, *Phys. Rev. B* **25**, 6049 (1982).

²⁸K. Morigaki, S. Toyotomi, and Y. Toyotomi, *J. Phys. Soc. Jpn.* **31**, 511 (1971); V. Ya Bratus, I. M. Zaritskii, G. S. Pekar, L. I. Khandros, and E. L. Shtrum, *Fiz. Tekh. Poluprovodn.* **14**, 1339 (1980) [*Sov. Phys.—Semicond.* **14**, 790 (1980)]; R. Romestain, *J. Phys. C* **13**, 1097 (1980). See also the discussion of hyperfine broadening of the ODMR lines in ZnO, C. Gonzalez, D. Block, R. T. Cox, and A. Hervé, *J. Cryst. Growth* **59**, 357 (1982), and the ODENDOR (Optically Detected Electron Nuclear Double Resonance) studies of shallow donors in CdS, ZnS, and ZnSe, J. J. Davies, J. E. Nicholls, and R. P. Barnard, *J. Phys. C* **18**, L93 (1985).

²⁹J. L. Merz, *Phys. Rev. B* **9**, 4593 (1974).

³⁰G. F. Neumark, *J. Lumin.* **31/32**, 512 (1984).

³¹R. J. Elliott, in *Polarons and Excitons*, edited by C. G. Kuper and G. D. Whitfield (Oliver and Boyd, Edinburgh, 1963), p. 269.

- ³²G. Fishman, *Ann. Phys. (Paris)* **5**, 5 (1980).
- ³³G. Fishman (private communication).
- ³⁴R. Bonneville and G. Fishman, *Phys. Rev. B* **22**, 2008 (1980).
- ³⁵F. Thuselet and K. Unger, *Phys. Status Solidi B* **79**, K39 (1977).
- ³⁶R. Bindemann, doctoral dissertation, Karl-Marx University, Leipzig, 1973 (unpublished); R. Bindemann and K. Unger, *Phys. Status Solidi B* **66**, 133 (1974). Some other authors using formulas having the form of Bindemann's equation state that such formulas are approximations only. However, Eq. (24) appears to us to be exact for finite r .
- ³⁷J. J. Hopfield and D. G. Thomas, *Phys. Rev.* **122**, 35 (1961).
- ³⁸See, e.g., A. M. Stoneham and A. H. Harker, *J. Phys. C* **8**, 1109 (1975); E. Kartheuser, R. Evrard, and F. Williams, *Phys. Rev. B* **21**, 648 (1980).
- ³⁹See, e.g., J. H. Jefferson, W. E. Hagston, and H. H. Sutherland; *J. Phys. C* **8**, 3457 (1975); E. Kartheuser, A. Babcenco, and R. Evrard, *Phys. Status Solidi B* **109**, 375 (1982); R. Englisch, *ibid.* **118**, 605 (1983).
- ⁴⁰C. H. Henry and K. Nassau, *Phys. Rev. B* **2**, 997 (1970).
- ⁴¹C. A. Arguello, D. L. Rousseau, and S. P. S. Porto, *Phys. Rev.* **181**, 1351 (1969).
- ⁴²D. Berlincourt, H. Jaffe, and L. Shiozawa, *Phys. Rev.* **129**, 1009 (1963).
- ⁴³A. S. Barker and J. C. Summers (unpublished data cited in Ref. 40).